Single-column modeling of the difference between the response of forest and grassland surface energy fluxes to heat waves

Lennert B. Stap (3137902)

Utrecht University
Institute for Marine and Atmospheric research Utrecht (IMAU)
Royal Netherlands Meteorological Institute (KNMI)

Supervisor: Prof. Dr. B.J.J.M van den Hurk (IMAU, KNMI)
Co-supervisor: Dr. R.A.J. Neggers (KNMI)

28 June 2012

Abstract

Observations have shown that differences in surface energy fluxes over grasslands and forests are amplified during heat waves (Teuling et al. 2010). The role of land atmosphere feedbacks in this process in still uncertain.

In this study, we use the single-column model (SCM) RACMO SCM to investigate the difference between forest and grassland in their energy response to heat waves. We have done three runs for the period 2005-2011: a control run by using the settings for Cabauw, the Netherlands, a run where the vegetation is changed to 100% forest and a run with 100% short grass as vegetation. The surface evaporation tendency equation developed by Van Heerwaarden et al. (2010) is used to analyse the impact of the land atmosphere feedbacks on evapotranspiration and sensible heat release in these two situations. A comparison is made with offline runs of the land scheme TESSEL, with the same settings, forced by atmospheric variables obtained from the outcomes of the reference Cabauw run of the SCM.

The expectation was that land atmosphere feedbacks amplify the difference in surface energy fluxes between forest and grass. The surface resistance feedback should have the largest impact, since the surface resistance is the factor that is changed by the vegetation kind. Using the surface evaporation tendency equation applied to the results of the SCM, we found that this is indeed the case. This resulted in higher air temperatures and earlier onsets of heat waves over forest, that tend to evaporate less.

Since planetary boundary layer feedbacks are not effective in the offline TESSEL runs, the amplified difference between forest and grassland during heat waves should be smaller than in the coupled SCM runs. This was found to be true. On a daily scale it was expected that if the feedbacks are more positive (negative) for grassland, the difference in evapotranspiration in the SCM results should be larger (smaller) than in the results of TESSEL. This behaviour was not present due to the effect of the feedbacks on the gain factors of the forcings and feedbacks, primarily via the surface resistance.

Contents

Chapter 1

Introduction

The projected increase in frequency, intensity and duration of heat waves in Europe (IPCC 2007) has severe socio-economic effects. Better understanding and predictability of heat waves is therefore of great importance. Earlier studies, e.g. Zaitchik et al. (2006) and Teuling et al. (2010), have focused on observed differences between vegetation kinds in energy distribution over sensible and latent heat release during heat waves. These differences have consequences for the atmospheric temperature profile and hence affect the duration and intensity of the heat wave. Fischer et al. (2007) and Van Heerwaarden et al. (2010) have investigated the influence of modeled land atmosphere feedbacks on evapotranspiration and temperature. In this study, we use a single-column model and an offline land scheme to analyse the influence of land atmosphere feedbacks on the modeled difference between forests and grasslands in excess surface energy partitioning over sensible and latent heat release during heat waves.

The earth surface can lose heat in three ways: via radiation, turbulent fluxes, namely the sensible heat flux and latent heat flux, and via the ground heat flux. As the sensible heat flux (H) warms the atmosphere, while the latent heat flux (LE) moistens it, the ratio between these two fluxes, known as the Bowen ratio (H/LE), influences the atmospheric temperature and its vertical structure.
Evapotranspiration is controlled by two variables: energy and soil moisture. When the maximum evaporative fraction (EF_{max}), the fraction of net surface radiation (R_{net}) that is used for evapotranspiration (LE/R_{net}), is reached, evapotranspiration is energy limited and we are in the wet soil moisture regime. When this is not the case, the evapotranspiration is soil moisture limited. If no evapotranspiration takes place at all, the soil moisture regime is called dry. Inbetween the dry and the wet regime lies the transitional regime (Figure 1.1). Different vegetation types account for different maximum evaporative fractions via regulation of the stomatal apertures and the area of the ground covered by their transpiring parts (Kelliher 1995). This affects the Bowen ratio.

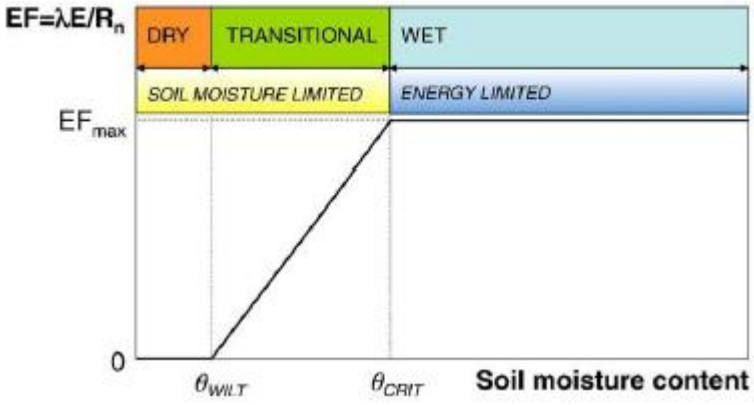

Figure 1.1: *Figure from Seneviratne et al. (2010). Definition of soil moisture regimes and corresponding evapotranspiration regimes.*

Teuling et al. (2010) observed a difference in the energy response to heat waves between grasslands and forests. An analysis of a network of flux towers in Europe revealed that grasslands tend to use the excess received energy during heat waves mostly for evapotranspiration/latent heat release, while forests are more conservative with their water content and use the energy mostly for sensible heat release. The resulting higher atmospheric temperatures will onset heat waves earlier over forests and make them more intense at the beginning. However, as the heat wave continues, it is anticipated that grasslands dry out earlier, so that heat waves are prolonged. Evapotranspiration is the determining factor in this difference between vegetation kinds.

Evapotranspiration can be determined with the Penman-Monteith equation. This equation is used in models by many meteorological organizations around the world, although the Royal Netherlands Meteorological Institute (KNMI) favours the Makkink method. It describes evapotranspiration as a function of available net radiation (net radiation minus ground heat flux), the vertical profile of atmospheric temperature and specific humidity and the vegetation. A change in latent heat flux alters the surface energy balance and hence the vertical profile of atmospheric temperature and specific humidity. This establishes the notion of land atmosphere feedbacks: a two-way coupling of a land quantity and an atmospheric quantity (Seneviratne et al. 2010).

The Penman-Monteith equation was used by Van Heerwaarden et al. (2010) to analyze the daily cycle of evaporation with a conceptual atmospheric boundary layer model on certain days in Cabauw (The Netherlands) and Niamey (Niger). These places represent mid-latitudes and semi-arid regions respectively. Van Heerwaarden et al. (2010) developed a time-derivative of the Penman-Monteith equation, which enabled him to distinguish the effects of forcings and feedbacks on evapotranspiration.

In this study, we use a single-column model (SCM) to study the response to heat waves of two different vegetation kinds (grassland and forest). An atmospheric model generally consists of a horizontal grid of vertical columns interacting with each other. A single vertical column of an atmospheric model can be run in a stand-alone mode, driven or controlled from the boundaries by external forcings. This is called single-column modelling. At KNMI a testbed for comparison of single-column models with Large Eddy Simulation (LES) and

observation data is established ([25], Neggers et al. 2012). The advantage of using a SCM over 3D-modelling is that is saves time, computational power and storing capacity while it is still able to accurately represent relevant processes and interactions in a controlled environment.

The SCM used at the KNMI is the RACMO SCM, with the Tiled ECMWF Scheme for Surface Exchanges over Land (TESSEL) as land scheme. TESSEL can also be run offline, for instance using RACMO SCM results as atmospheric forcing. Comparison between offline land scheme runs and coupled land atmosphere SCM runs enables the quantification of the importance of land atmosphere feedbacks.

In the present thesis, runs of TESSEL and RACMO SCM, are done over the 7 year period 2005-2011 for Cabauw. Different runs are done, with as vegetation grass, forest and the actual vegetation of Cabauw. Investigated is the reaction of the surface energy balance terms of the different vegetation types to heat waves. Of particular interest is the consequence of the different reactions for the intensity and duration of the heat wave. The tendency equation for surface evaporation derived by Van Heerwaarden et al. (2010) gives a framework to analyse forcings and feedbacks in the process of evapotranspiration. During heat waves, land atmosphere feedbacks are expected to increase the difference in evapotranspiration between grassland and forest. Land atmosphere feedbacks are not represented in the runs with the offline land scheme. Coupled land-atmosphere modelling with the SCM should therefore perform better in matching observations.

TESSEL and RACMO SCM are described in Section 2.1. Section 2.2 deals with the tendency equation for surface evaporation developed by Van Heerwaarden et al. (2010). The numerical experiments done with TESSEL and RACMO SCM are explained in Section 2.3. In Chapter 3 the results can be found. First the SCM is validated against measurements and the outcomes of the uncoupled TESSEL runs (Section 3.1). Next, the integrated energy response to heat waves is quantified for the offline TESSEL runs and the runs of the SCM (Section 3.2). The daily evaporation cycle during a selected non-heat wave, early heat wave and late heat wave day for both vegetation kinds is discussed in Section 3.3. The differences in turbulent fluxes, temperature and feedbacks between forest and grassland are the focus of Section 3.4. These differences are depicted as a function of incoming radiation and soil moisture content. A conclusion, along with a discussion of the results and research perspectives, is presented in Chapter 4.

Chapter 2

Model and methods

In this Chapter we give a description of TESSEL and RACMO SCM. The tendency equation for surface evaporation developed by Van Heerwaarden is presented. Finally, we explain the numerical experiments that are done and the method of analyzing the results.

2.1 Modeling surface evaporation

2.1.1 TESSEL

The Tiled ECMWF Scheme for Surface Exchanges over Land (TESSEL) is a second-generation land surface model (Seneviratne 2010). It explicitly models 20 different vegetation kinds (Van den Hurk 2000) of which short grass and evergreen needleleaf trees are of interest to this study. Vegetation is modeled via the leaf area index (LAI), minimum surface resistance ($r_{s,min}$), VPD correction factor for $r_{s,min}$ (g_d), root distribution over the soil layers (R) and thermal conductivity of the skin layer (Λ_s) (Table 2.1).

TESSEL divides each surface grid cell into 6 land and 2 water fractions, or tiles (Figure 2.1): high vegetation, low vegetation, bare soil, snow on bare soil/low vegetation, snow under high vegetation and interception reservoir on land and ocean/lakes and sea-ice on water.

Evapotranspiration comes from four sources: vegetation, bare soil, the interception layer and snow sublimation. We are interested in the difference in evapotranspiration between grassland and forest and so only evapotranspiration from vegetation is considered here.

TESSEL has 4 soil model levels of depths 7 cm, 21 cm, 72 cm and 189 cm. Each layer i has a moisture content $q_{soil,i}$ and temperature $T_{soil,i}$. The fraction of roots located in each layer differs per vegetation type (Table 2.1).

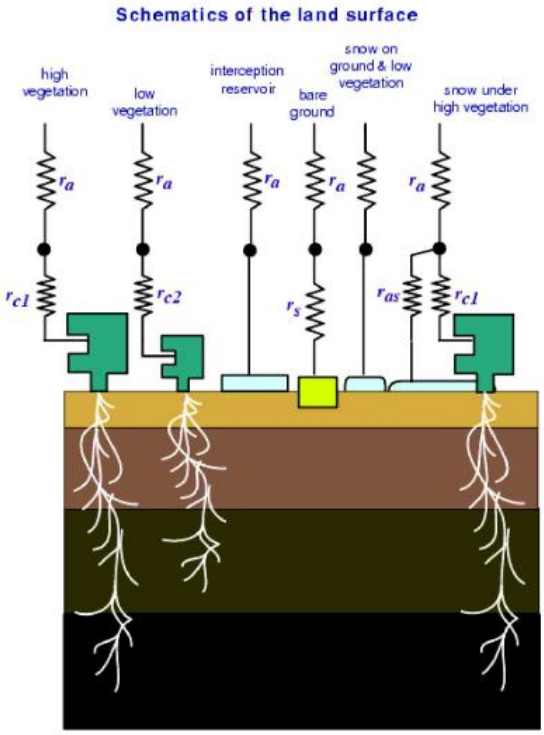

Figure 2.1: *Figure from Van den Hurk et al. (2000). Grid cell tiles on the land, used by TESSEL.*

Surface energy balance

In a snowfree environment the surface energy balance (SEB) can be expressed as:

$$R_{net} = H + LE + G. \tag{2.1}$$

with H the sensible heat flux, LE the latent heat flux and G the ground heat flux, all defined positive away from the surface.

Net surface radiation R_{net} is the difference between the incoming and outgoing short wave and long wave radiation fluxes:

$$R_{net} = S_{in} - S_{out} + L_{in} - L_{out}. \tag{2.2}$$

The incoming fluxes are defined positive downward, the outgoing fluxes positive upward.

With the Stefan-Boltzmann law and the definition of albedo α as the ratio of outgoing over incoming short wave radiation, we can write:

$$R_{net} = (1 - \alpha)S_{in} + L_{in} - \sigma T_s^4, \tag{2.3}$$

with σ the Stefan-Boltzmann constant and T_s the surface temperature.

For each tile TESSEL solves the SEB for T_s, as all the terms are explicitly or implicitly dependent on this variable. The final solution for a grid cell is an area weighed average of the tile solutions.

Table 2.1: *Properties of the land surface, used by TESSEL.*

variable	description (unit)	forest	grassland
LAI	Leaf area index (m^2m^{-2})	5	2
$r_{s,min}$	Minimum surface resistance (sm^{-1})	500	110
g_d	VPD correction factor for r_s (hPa^{-1})	0.03	0
R_1	Fraction of roots in soil layer 1 (%)	26	35
R_2	Fraction of roots in soil layer 2 (%)	39	38
R_3	Fraction of roots in soil layer 3 (%)	29	23
R_4	Fraction of roots in soil layer 4 (%)	6	4
Λ_s	Thermal conductivity skin layer ($Wm^{-2}K^{-1}$)	20	10
w_{wilt}	Volumetric water content at wilting point (m^3m^{-3})	0.171	0.171
w_{fc}	Volumetric water content at field capacity (m^3m^{-3})	0.323	0.323

Latent heat flux
TESSEL calculates the latent heat flux from vegetation as:

$$LE = \frac{\rho L_v}{r_a + r_s}(q_{sat}(T_s) - q), \tag{2.4}$$

with r_a and r_s the aerodynamic and surface resistance, ρ the density of the atmosphere near the surface, at the lowest model level (see Section 2.1.2), L_v the latent heat of vaporization, $q_{sat}(T_s)$ the saturated specific humidity inside the canopy and q the humidity at the lowest half level of the model, located at the surface. Evapotranspiration E follows from:

$$E = LE/L_v. \tag{2.5}$$

Aerodynamic resistance
The aerodynamic resistance r_a is obtained by:

$$\frac{1}{r_a} = Uk^2 \left[\ln\left(\frac{z_{sl}}{z_{0m}}\right) - \Phi_M\left(\frac{z_{sl}}{L}\right) + \Phi_M\left(\frac{z_{0m}}{L}\right)\right]\left[\ln\left(\frac{z_{sl}}{z_{0h}}\right) - \Phi_H\left(\frac{z_{sl}}{L}\right) + \Phi_H\left(\frac{z_{0h}}{L}\right)\right], \tag{2.6}$$

with k the Von Kármán constant, U the wind speed at the lowest half level of the model and z_{0m} and z_{0h} the roughness lengths for momentum and heat. The depth of the surface layer z_{sl} is defined as the sum of z_{0m} and the height of the lowest model level.

Monin-Obukhov length L is defined as:

$$L = \frac{u_*^3}{k\frac{g}{T}\overline{(w'\theta')}_s} \tag{2.7}$$

where g is the gravitational constant, T is temperature of the lowest model level and $\overline{(w'\theta')}_s$ the sensible heat flux at the lowest model half level (located at the surface).

Friction velocity u_* is given by:

$$u_* = \frac{\mid \tau_{\mathbf{R}} \mid}{\rho}, \tag{2.8}$$

with $\mid \tau_{\mathbf{R}} \mid$ the Reynolds stress at the surface.

The integrated stability functions for momentum Φ_M and heat Φ_H are:

$$\Phi_M(z) = \frac{\pi}{x} + 2\arctan x + \log\frac{(1+x)^2 \cdot (1+x^2)}{8} \text{ and} \tag{2.9}$$

$$\Phi_H(z) = 2\log\frac{1+x^2}{2} \tag{2.10}$$

in unstable conditions (z/L<0), with $x = (1 - 16\frac{z}{L})^{1/4}$. In stable conditions ($z/L$>0) they read:

$$\Phi_M(z) = -b(\frac{z}{L} - \frac{c}{d})\exp -d\frac{z}{L} - a\frac{z}{L} - \frac{bc}{d} \text{ and} \tag{2.11}$$

$$\Phi_H(z) = -b(\frac{z}{L} - \frac{c}{d})\exp -d\frac{z}{L} - (1 + \frac{2}{3}a\frac{z}{L})^{1.5} - \frac{bc}{d} + 1 \tag{2.12}$$

with $a = 1$, $b = 2/3$, $c = 5$, $d = 0.35$.

Surface resistance

Following the method of Jarvis (1976), the surface resistance is parametrized as a function of incoming short wave radiation at the surface S_{in}, volumetric soil moisture content w and water vapour deficit VPD:

$$r_s = \frac{r_{s,min}}{LAI} f_1(S_{in}) f_2(w) f_3(VPD), \tag{2.13}$$

with $r_{s,min}$ as the minimum surface resistance and LAI the leaf-area index (both dependent on the vegetation type, see Table 2.1). LAI is defined as the area of leaves of the surface area.

The volumetric water content is calculated as:

$$w = \sum_{k=1}^{4} w_k * R_k, \tag{2.14}$$

with w_k the watercontent of the kth layer in mm and R_k the fraction of roots in the kth layer (see Table 2.1).

The water vapor deficit follows from:

$$VPD = e_s(T) - e, \tag{2.15}$$

with $e_s(T)$ the saturation water vapor pressure and e the water vapor pressure, both at the lowest level of the model.

The functions used in equation 2.13 are:

$$\frac{1}{f_1} = (1, \frac{0.004S_{in} + 0.05}{0.81(0.004S_{in} + 1)}), \tag{2.16}$$

$$\frac{1}{f_2} = \begin{cases} 0 & \text{if } w < w_{wilt} \\ \frac{w - w_{wilt}}{w_{fc} - w_{wilt}} & \text{if } w_{wilt} \leq w \leq w_{fc} \\ 1 & \text{if } w > w_{fc} \end{cases} \tag{2.17}$$

$$\frac{1}{f_3} = \exp(-g_d VPD). \tag{2.18}$$

In these equations w_{wilt} is the soil moisture at permanent wilting point, w_{fc} is the soil moisture at field capacity and coefficient g_d dependent on the vegetation type (see Table 2.1).

Sensible heat flux and ground heat flux
TESSEL calculates the sensible heat flux as:

$$H = \frac{\rho c_p}{r_a}(\theta_s - \theta), \tag{2.19}$$

where c_p is the heat capacity of air at constant pressure and θ_s and θ are the potential temperatures of the surface and the lowest model level.

The ground heat flux is obtained by:

$$G = \Lambda_s(T_s - T_{soil1}), \tag{2.20}$$

with Λ_s the thermal conductivity of the skin layer, dependent on the tile (Table 2.1) and T_{soil1} the temperature over the upper layer of the soil.

Penman-Monteith equation
Combining equation 2.4 and 2.19 with the SEB, linearizing $q_{sat}(T)$ and eliminating surface temperature leads to:

$$LE = \frac{\frac{dq_{sat}}{dT}(R_{net} - G) + \frac{\rho c_p}{r_a}(q_{sat}(T) - q)}{\frac{dq_{sat}}{dT} + \frac{c_p}{L_v}\left(1 + \frac{r_a}{r_s}\right)}, \tag{2.21}$$

the well-known Penman-Monteith equation (Monteith 1965).

2.1.2 KNMI SCM

The single-column model (SCM) used in this study is that of the Regional Atmospheric Climate Model (RACMO, Van Meijgaard et al. 2008). The SCM is forced by so-called driver files, which contain the initial conditions, boundary conditions and external forcings that are required to perform an SCM simulation. The driver files are generated from daily 72-hour forecasts with the RACMO 3D model, performed on a domain that contains Europe, for which the initial and boundary conditions are obtained from the ECMWF (European Centre for Medium-range Weather Forecasts) analysis and forecasts. The SCM couples the TESSEL land scheme to the atmospheric model, the latter being discretized at the standard 91-level configuration of the currently operational Integrated Forecast System (IFS) of the ECMWF. At these model levels the atmospheric state variables such as temperature, humidity and momentum are calculated. The pressure is determined at each half level, dependent on the surface pressure. The boundary layer scheme for transport and clouds as used in this study is described in detail by Neggers et al. (2009a, 2009b). The remainder of the sub-grid physics of the RACMO SCM is identical to that of cycle 31r1 of the IFS (documentation available online [26]).

The setup of the SCM simulations as adopted here is described in detail by Neggers et al. (2012). Reflecting the RACMO setup the SCM simulations are also performed in a staggered mode, each lasting 36 hours. Only day one of the simulation is evaluated. The series of SCM simulations can thus cover multiple years, as described in detail in Section 2.3. The timestep of the SCM simulation is always 900 s, reflecting the operational IFS.

2.2 A tendency equation for surface evapotranspiration

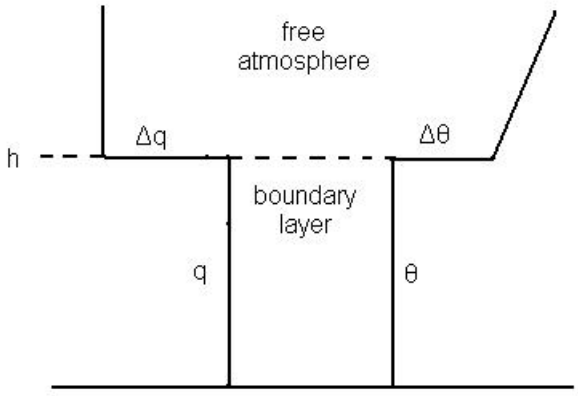

Figure 2.2: *Sketch of the specific humidity and potential temperature profile assumed in the mixed-layer model. Symbols explained in the text.*

The conceptual model used by Van Heerwaarden et al. (2010) assumes one value for the potential temperature and specific humidity for the whole boundary layer and jumps of these variables ($\Delta\theta$, Δq) at the boundary layer top (sketched in Figure 2.2), originating from the mixed-layer model of Tennekes (1973). The evolution of temperature and specific humidity can then be descibed as:

$$\frac{dT}{dt} = \frac{d\theta}{dt} = \frac{1}{h}\left(\frac{H}{\rho c_p} + w_e \Delta\theta\right) + adv_\theta, \tag{2.22}$$

$$\frac{dq}{dt} = \frac{1}{h}\left(\frac{LE}{\rho L_v} + w_e \Delta q\right) + adv_q, \tag{2.23}$$

with w_e the entrainment velocity, h the boundary layer height and adv_θ and adv_q the advection of potential temperature and specific humidity respectively. If we now in succession differentiate the Penman-Monteith equation (Equation 2.21) in time, group all the terms per tendency, replace $R_{net} - G - LE$ by H (Equation 2.1) and apply equations 2.22 and 2.23, we obtain:

$$\begin{aligned}
\frac{dLE}{dt} &= c_0 \frac{dq_{sat}}{dT}\left((1-\alpha)\frac{dS_{in}}{dt} + \frac{dL_{in}}{dt}\right) \\
&+ c_0\left(H\frac{d^2 q_{sat}}{dT^2} + \frac{\rho c_p}{r_a}\frac{dq_{sat}}{dT}\right) adv_\theta - c_0 \frac{\rho c_p}{r_a} adv_q \\
&+ c_0\left(H\frac{d^2 q_{sat}}{dT^2} + \frac{\rho c_p}{r_a}\frac{dq_{sat}}{dT}\right)\left\{\frac{H}{\rho c_p h} + \frac{w_e \Delta\theta}{h}\right\} - c_0 \frac{\rho c_p}{r_a}\left\{\frac{LE}{\rho L_v h} + \frac{w_e \Delta q}{h}\right\} \\
&- c_0\left(\frac{\rho c_p}{r_a^2}(q_{sat} - q) - LE\frac{c_p}{L_v}\frac{r_s}{r_a^2}\right)\frac{dr_a}{dt} \\
&- c_0 \frac{dq_{sat}}{dT}\frac{dL_{out}}{dt} - c_0 \frac{dq_{sat}}{dT}\frac{dG}{dt} - c_0 LE \frac{c_p}{L_v}\frac{1}{r_a}\frac{dr_s}{dt},
\end{aligned} \tag{2.24}$$

with

$$c_0 = \frac{1}{\frac{dq_{sat}}{dT} + \frac{c_p}{L_v}\left(1 + \frac{r_s}{r_a}\right)}. \tag{2.25}$$

henceforward the Van Heerwaarden equation (Van Heerwaarden 2010). This equation seperates the external forcings of evapotranspiration, from the feedbacks. A feedback is a two way coupling of two variables. This means that a process is modified by its results or effects. So, in this case, a change in evapotranspiration by external forcing leads to a change in another variable, which impacts on evapotranspiration.
Represented in the Van Heerwaarden equation are:

Surface radiation forcings (*line 1*)
Radiation forces evapotranspiration. These terms represent the effects of variations in the incoming solar (via $\frac{dS_{in}}{dt}$) and planetary (via $\frac{dL_{in}}{dt}$) radiation. Both terms are positively related to the evaporation tendency, because more radiation generally leads to more evapotranspiration.

Boundary layer forcings (*line 2*)
In the boundary layer advection of heat and moisture takes place. Advected heat leads to more evapotranspiration, while advected moisture acts negatively on evapotranspiration by decreasing the ability of the atmosphere to take up moisture.

Boundary layer feedbacks (*line 3*)
In the boundary layer the latent heat and sensible heat flux impact on evapotranspiration. The height of the boundary layer is impacted by entrainment. We distinguish four feedbacks:

1. Surface warming feedback (first term, first term in brackets):

$$\boxed{H \uparrow} \rightarrow \boxed{\theta \uparrow} \rightarrow \boxed{LE \uparrow} \rightarrow \boxed{H \downarrow} \tag{2.26}$$

   Sensible heat warms up the atmosphere, which will increase its ability to take up moisture. This will lead to more evapotranspiration, which will limit the amount of energy available for sensible heat release.

2. Entrainment warming feedback (first term, second term in brackets):

$$\boxed{h \uparrow} \rightarrow \boxed{\theta \uparrow} \rightarrow \boxed{LE \uparrow} \rightarrow \boxed{H \downarrow} \rightarrow \boxed{h \downarrow} \tag{2.27}$$

   Entrainment of warm air at the top of the boundary layer will also warm up the boundary layer and thereby increase its water demand. This leads to increased evapotranspiration. Consequently sensible heat release is reduced, slowing down the boundary layer growth.

3. Surface evaporation feedback (second term, first term in brackets):

$$\boxed{LE \uparrow} \rightarrow \boxed{q \uparrow} \rightarrow \boxed{LE \downarrow} \tag{2.28}$$

   Evapotranspiration will increase the amount of moisture in the atmosphere, limiting its ability to take it up.

4. Entrainment drying feedback (second term, second term in brackets):

$$\boxed{q\uparrow} \rightarrow \boxed{LE\downarrow} \rightarrow \boxed{H\uparrow} \rightarrow \boxed{h\uparrow} \rightarrow \boxed{q\downarrow} \tag{2.29}$$

   Entrainment of dry air at the top of the boundary layer will increase the amount of moisture in the atmosphere as well, thereby reducing evapotranspiration. This will increase sensible heat release and consequently boundary layer growth.

The temperature related processes (feedback 1 and 2) act positively on evapotranspiration, because a warmer atmosphere can take up more moisture. The moisture related processes on the other hand work negatively, because more moisture in the atmosphere limits its ability to take it up. All the closed feedbacks are negative, because the perturbed variable is pushed back to its original state. The boundary layer feedbacks are neatly described in Van Heerwaarden et. al. (2009) (see Figure 2.3).

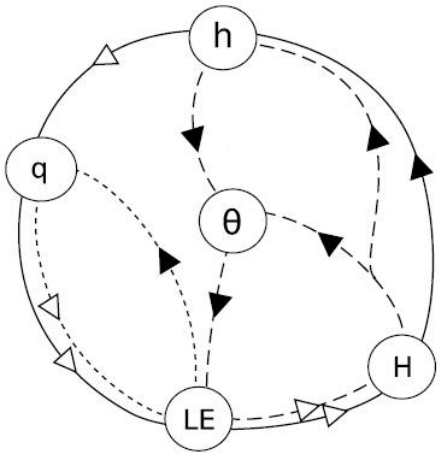

Figure 2.3: *Figure from Van Heerwaarden et al. (2009). Schematical overview of the boundary layer feedbacks. Closed arrows respresent a positive coupling, open arrows a negative coupling. Symbols explained in the text.*

Surface layer feedback (*line 4*)
This term represents the surface layer process. If the aerodynamic resistance increases, evapotranspiration is hindered. This consequently decreases the stability of the atmosphere, which decreases the aerodynamic resistance.

Land surface feedbacks (*line 5*)
Three land surface processes play a role in the daily cycle of evapotranspiration. Long wave radiation (first term) and ground heat flux (second term) will limit the amount of energy available for latent heat release. An increase in surface resistance (third term), due to strengthened incoming radiation, soil drying or VPD increase, leads to less evapotranspiration. The vapour pressure deficit is then compensated less and less soil moisture is used. This will impact negatively on the surface resistance.

Diagnostics in RACMO SCM
RACMO SCM differs from the conceptual model of Van Heerwaarden et al. (2010) in that it does not have a priori well mixed temperature and specific humidity profiles. These quantities are determined for each layer seperately. T is diagnosed from the RACMO SCM results as the surface value, q as the value at the lowest model level. For $w_e\Delta\theta$ the minimal value of the turbulent flux of dry static energy is used, divided by c_p and ρ. Boundary layer height h is assumed to be the height at which this minimum occurs. Hereafter, $w_e\Delta q$ is the turbulent flux of water vapour at this height. Finally, cubic smoothing splines are fitted through the incremental data of $w_e\Delta\theta$, $w_e\Delta q$ and h (all being defined discretely at model heights). The smoothed values are used in all the feedback calculations.
In RACMO SCM cloud cover is calculated, while this is not the case in the conceptual model. Clouds alter incoming radiation: shortwave incoming radiation is decreased, while longwave incoming radiation is increased. This will affect evapotranspiration, which in turn will change cloud cover (the effect depends on evaporative and nonevaporative processes (Ek and Holtslag 2004)). This feedback is not taken in account in this study.

2.3 Numerical experiments

Model runs
The SCM is configured to replicate the settings at Cabauw, the Netherlands. Cabauw is a grassland station, operated by KNMI. It is located 51.971° N, 4.927° E and 0.7 m below sea level. The nearby region is agricultural, and surface elevation changes are at most a few metres over 20 km (van Ulden and Wieringa 1996). Observations from the site are stored in the CESAR (Cabauw experimental site for atmospheric research) database. They are large in quantity and easily accessible. First, the coupled model is run using these settings (Table 2.2, Cabauw).

Cabauw was one of the places that Teuling et al. (2010) analyzed. He compared it Loobos, a nearby forest site. However, the model allows us to make Cabauw a total grassland site and a total forest site by changing the high/low vegetation cover and the albedo (Table 2.2, forest and grassland). This enables us to isolate the effects of vegetation. For grassland we have chosen short grass and for forest we have chosen evergreen needleleaf trees, because these are the vegetation types that are normally present at Cabauw. The model is also run using these settings.

Table 2.2: *Properties of the land surface, used in the different runs of the single-column model.*

variable (unit)	Cabauw	forest	grassland
latitude (° N)	51.89075	51.89075	51.89075
longitude (° E)	4.817139	4.817139	4.817139
high vegetation cover (%)	1.489258	100	0
low vegetation cover (%)	79.6875	0	100
albedo (-)	0.1858447	0.16	0.20

Next, we use the results of the Cabauw run (near surface values for temperature, specific humidity and wind, surface pressure, incident short wave and long wave radiation and the rainfall and snowfall rate) to force the uncoupled TESSEL land scheme, set up with the same initial values as the coupled model run. In the same way as with the coupled model, we do three runs: one with the actual vegetation of Cabauw, one with grassland and one with forest as vegetation.

All the runs are done for the period 1 January 2005 to 31 December 2011, in which three heat waves were recorded in the Netherlands by the KNMI: 18 June 2005 to 24 June 2005 (7 days), 30 June to 6 July (7 days) and 15 July to 30 July 2006 (16 days)[27]. This period is very recent, so it is representative for present conditions. It is long enough to calculate normal summer conditions and analyze heat wave conditions. Observations were easily available and done with accurate, modern equipment. Both the coupled SCM and the offline land scheme gave 15-minute values for all variables.

Analysis

To evaluate the model results, energy, temperature and precipitation data from the CESAR database are compared to the coupled Cabauw run (Section 3.1). This run is also compared to the uncoupled Cabauw run. These runs should give the same results, as they were forced in the same way. Any differences that occur can be attributed to the version of TESSEL used offline being newer then the one used in RACMO SCM. Although most of the new features are switched off in the offline run, the hydrologies of the cycles still differ slightly.

The coupled and uncoupled grassland and forest runs are used to analyze heat wave occurence, summer radiation flux climatology, and heat wave flux anomalies. We adopt the definition of a heat wave that the KNMI uses: at least 5 consecutive days with a maximum temperature of 25° C or higher, of which at least 3 days with a maximum temperature above 30° C (so-called 'tropical days'). It is expected that differences between grassland and forest in land atmosphere feedbacks increase the difference in flux anomalies on heat wave days. These feedback differences are not present in the offline TESSEL runs, that are both forced with the same atmospheric data. This would mean that coupled land atmosphere modeling performs better in representing heat waves than using a land scheme only.

Next, for three cloudless days representing a normal summer day, an early heat wave day and a late heat wave day, the different terms in the Van Heerwaarden equation are investigated. Differences in forcings and feedbacks between the days, and between the vegetation types are analyzed. We try to explain the difference between the SCM runs and TESSEL runs on the daily scale by the feedback difference.

Finally, the integrated feedback difference is displayed as a function of incoming solar radiation and soil moisture content. This is done for the total feedback and all the feedbacks separately. In this way, a clear view of the effect of feedbacks on evapotranspiration and atmospheric temperatures in different environmental and atmospheric situations is given. Atmospheric temperatures are expected to be higher over forest because forest releases more sensible heat. This particularly happens in heat wave situations. However, as soil moisture gets depleted, this difference is expected to shrink.

Chapter 3

Results

This Chapter deals with the results of the numerical experiments. First, we validate RACMO SCM outcomes against observations and against the offline TESSEL results. Next, we analyze the integrated summer energy fluxes. For three days, representing an early heat wave day, a normal summer day and a late heat wave day, we investigate the daily cycle of evapotranspiration tendency. Finally, we explain the effect of the feedbacks on the latent heat flux and the effect of the latent heat flux on atmospheric temperature differences.

3.1 Model validation

Using the actual vegetation of Cabauw, the SCM output showed 4 heat waves in the period 2005-2011. The first was from 18 June to 25 June 2005 (8 days), the second from 30 June to 7 July 2006 (8 days), the third from 10 July to 30 July 2006 (21 days) and the last from 7 July to 15 July 2010 (9 days). This differs from the observed heat waves in De Bilt (Section 2.3). For the validation of the model, the modeled heat waves are taken to be heat waves for the observed quantities too. Observations of 2m temperature, precipitation and of the SEB terms are obtained online from the CESAR database ([28]).

3.1.1 SCM and observations

Mean temperature
The temperature at Cabauw is measured every 10 minutes with a KNMI Pt500-element in an unventilated KNMI temperature hut. Accuracy is 0.1 K, resolution is 0.1 K.

If we compare the modeled mean 2m air temperature to the observations for all summer days (JJA) in the period 2005-2011, the model has a warm bias of 0.56 K. The root mean square error (rmse) is 1.18 K and the correlation between the two datasets is 0.94. When we look only at heat wave days the bias grows to 1.01 K and the rmse to 1.30 K. We conclude that mean temperature is modeled accurately up to 1.5 K on short (daily) time scales.

Rain

The rain at Cabauw is measured every 10 minutes with the KNMI rain gauge. Accuracy is 0.2 mm, resolution is 0.1 mm.

Comparing measured rain amounts per day to modeled rain rates, the model shows a bias of -0.38 mm/day for all summer days in the period 2005-2011. The rmse is very high: 6.25 mm/day on an average rain amount of 3.24 mm/day. The correlation between the datasets is 0.51. Considering only heat wave days reduces the bias to -0.28 mm/day and the rmse to 5.81 mm/day. So heat wave days do not show worse deviations from the observations then normal summer days. In conclusion, on daily time scales rain is not modeled very accurately.

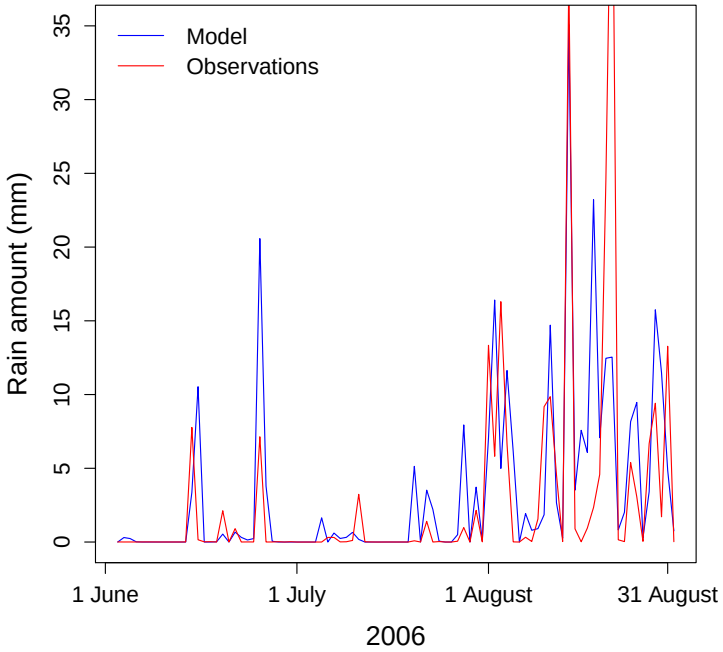

Figure 3.1: *Rain amount accumulated per day in the summer of 2006, as measured and modeled by the SCM at Cabauw.*

Table 3.1: *Accumulated summer rainfall, as measured and modeled by the SCM at Cabauw.*

summer	observed acc. rain amount (mm)	modeled acc. rain amount (mm)	relative difference (%)
2005	319	214	-33
2006	258	302	17
2007	432	321	-26
2008	237	249	5
2009	187	203	9
2010	269	266	-1
2011	385	285	-26

This improves if we consider longer time scales, such as the whole 2006 summer (Figure 3.1). We notice that model output and observations of periods of little rain and periods of much rain coincide within a few days. The model calculates a total rain amount of 301.5 mm, while 257.1 mm rain was observed during this summer, a deviation of only 17%. Table 3.1 shows for all summers the accumulative modeled and observed rain amount and the relative difference. The average absolute deviation per summer is 16.8% so we conclude that modeling of rain on longer (seasonal) time scale is accurate up to 20%.

Surface energy balance

For both the observations and the different models, the terms of the SEB are calculated for normal (non-heat wave) summer days. Following Teuling et al. (2010) the period 9.00-13.00 UTC is considered, when heating at the surface is maximal. The average of these days is considered the summer climatology (Figure 3.2). Also, the mean of the heat wave days (as calculated by the SCM) is calculated. If we subtract the climatology we get the heat wave day anomaly (Figure 3.3).

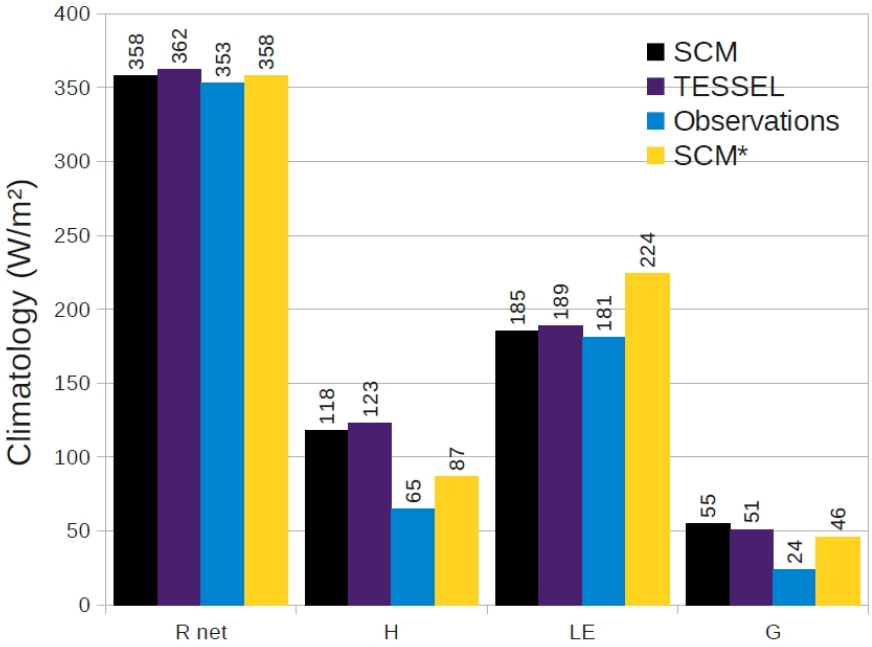

Figure 3.2: *Summer 9-13 UTC mean flux climatology over 2005-2011 for net radiation, sensible heat flux, latent heat flux and ground heat flux.*

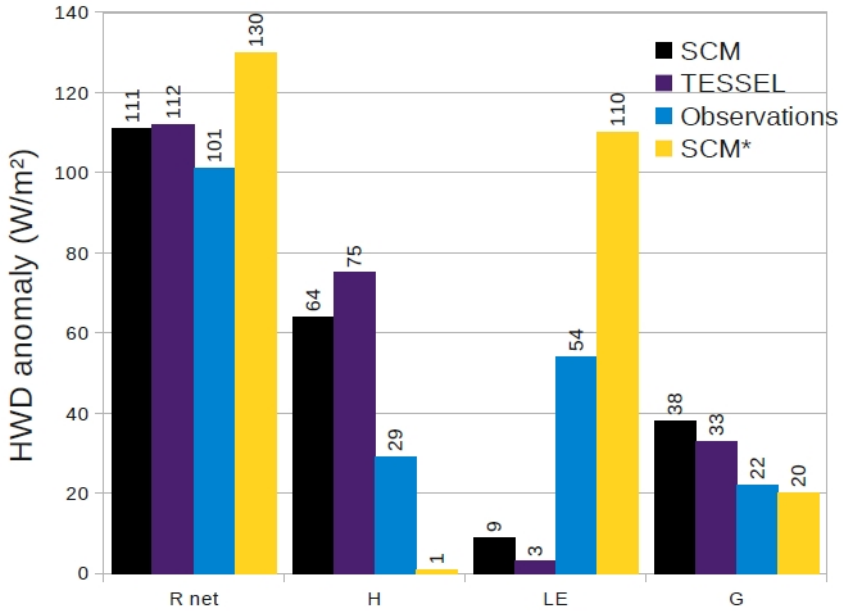

Figure 3.3: *Summer 9-13 UTC mean heat wave day anomaly over 2005-2011 for net radiation, sensible heat flux, latent heat flux and ground heat flux.*

Net radiation

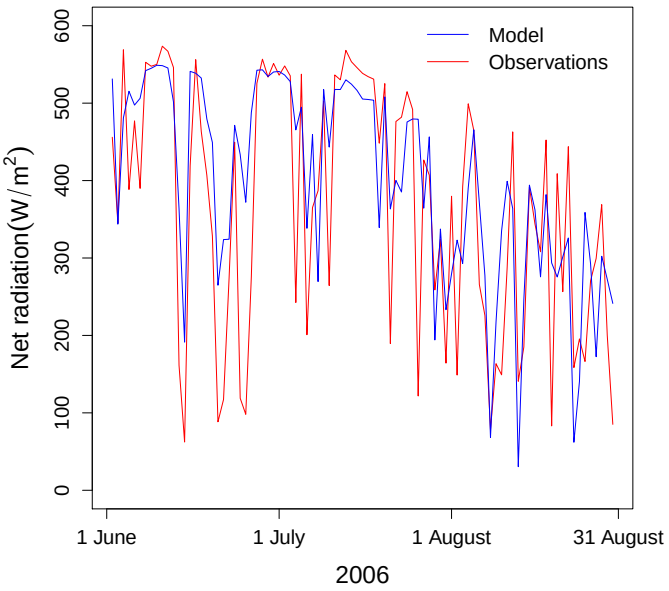

Figure 3.4: *Mean 9-13 UTC net incoming radiation in the summer of 2006, as measured and modeled by the SCM at Cabauw.*

Radiation is measured every 10 minutes at Cabauw. Kipp Zn CM11 pyranometers are used for short wave radiation. Long wave radiation is measured with Eppley pyrgeometers (PIR). The net radiation is obtained with equation 2.2.

On seasonal time scales the net radiation is well captured by the model (Figure 3.4), although the modeled net radiation shows less variability. This is most likely a consequence of less cloud formation. The modeled 9-13 UTC summer mean for 2005-2011 is 358 Wm^{-2} for non-heat wave days, with 353 Wm^{-2} observed. Heat waves show a modeled average of 469 Wm^{-2}, with 454 Wm^{-2} observed. This difference is mainly due to higher modeled surface temperatures, leading to increased outgoing longwave radiation.

On the daily scale the modeled net radiation agrees with the cycle of the observations (Figure 3.5). Differences can be attributed to measurement errors and cloud cover in the measurements. We conclude that radiation is modeled accurately.

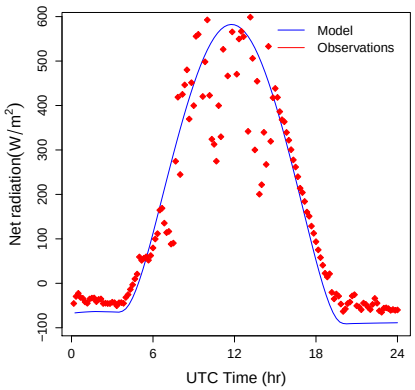

Figure 3.5: *Daily cycle of the net radiation at 15 June 2010, a typical cloudless summer day in the model output of the SCM, as measured and modeled by the SCM at Cabauw.*

Turbulent fluxes

At Cabauw turbulent fluctuations of wind, temperature, and humidity are measured every 10 minutes with a combination of a sonic anemometer/thermometer (wind vector and sonic temperature) and an optical open path sensor (water vapor). From this the vertical fluxes of sensible and latent heat are derived by means of the eddy correlation technique (Lee, Masman and Law 2004). The sonic anemometer is a Kaijo-Denki, probe type TR60-A, electronic unit DAT-300 or DAT-600. The sonic path is 0.2 m, resolution is 0.1 K. The water vapor-sensor is a KNMI Infrared Fluctuation Meter (IFM). Pathlength is 0.3 m, resolution is 0.003 g/m^3 H_2O.

On non-heat wave days the latent heat flux is slightly overestimated by the SCM: the modeled 9-13 UTC summer mean is 185 Wm^{-2}, while 181 Wm^{-2} is observed. On heat wave days an underestimation occurs: an average of 194 Wm^{-2} is modeled, while 235 Wm^{-2} is observed. Figure 3.6 shows large differences between the model and the observations in July, when there was a heat wave and the soil was very dry.

Table 3.2: *Bowen ratios of the climatology and the HWD average for the reference runs.*

	Climatology	HWD average
SCM	0.64	0.94
TESSEL	0.65	1.03
Observations	0.36	0.40
SCM*	0.39	0.26

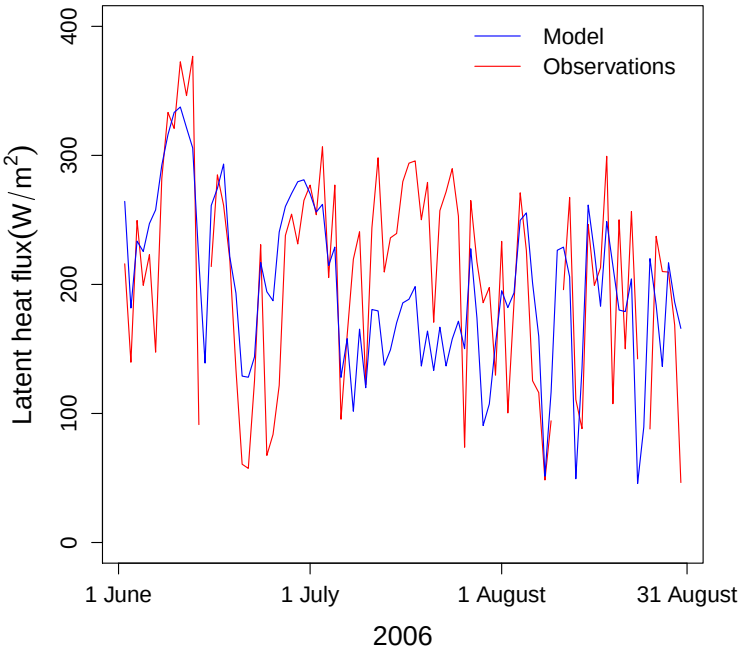

Figure 3.6: *Mean 9-13 UTC latent heat flux in the summer of 2006, as measured and modeled by the SCM at Cabauw.*

The contrary is true for the sensible heat flux (Figure 3.7). On non-heat wave days it is overestimated: the model value for the 9-13 UTC summer mean is 118 Wm^{-2}, with only 65 Wm^{-2} observed. The modeled Bowen ratio (H/LE) for non-heat wave days is 0.64, while only 0.36 is observed (Table 3.2).

However, the observed energy balance does not close. This energy balance closure problem is in accordance with the findings of Teuling et al. (2010) and well documented in the literature (e.g. Wilson et al. (2002) for an overview and Foken et al. (2006) for the influence of land surface heterogeneity). When the energy balance residual is added entirely to the sensible heat flux (green line in Figure 3.7), we get a 9-13 UTC summer mean of 150 Wm^{-2}, 27% more then the model calculates.

On heat wave days the overestimation of sensible heat flux by the model increases to 94%: 94 Wm^{-2} observed and 182 Wm^{-2} modeled. The average Bowen ratio of heat wave days is 0.94 for the modeled response and only 0.40 for the observations. Even adding the residual term to the sensible heat can no

longer compensate the deviation, as it gives a 9-13 UTC mean of 177 Wm^{-2} for heat wave days. This is shown by Figure 3.7 in July.

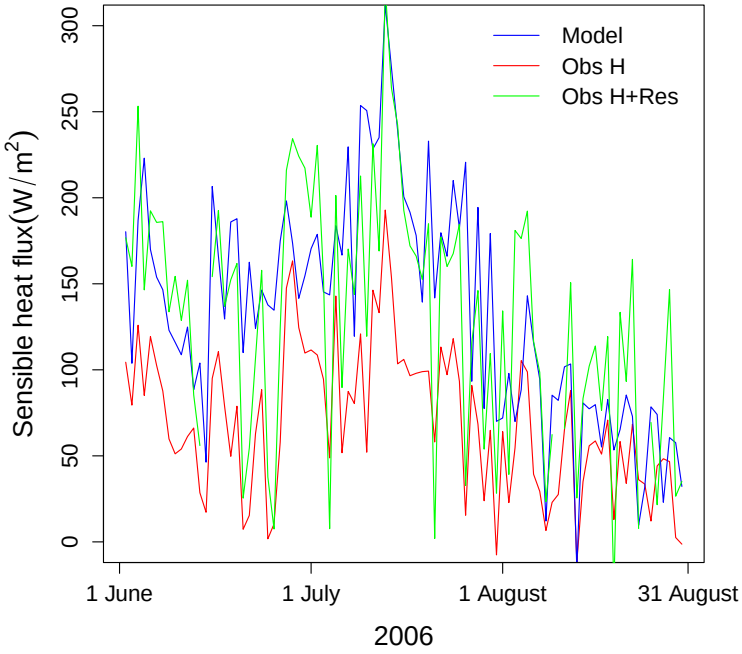

Figure 3.7: *Mean 9-13 UTC sensible heat flux in the summer of 2006, as measured and modeled by the SCM at Cabauw (Obs H) and the measured residual term added to the measured sensible heat (Obs H + Res)*

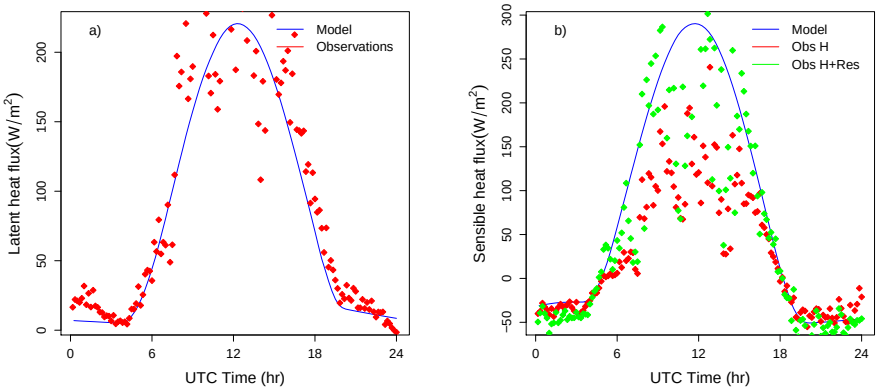

Figure 3.8: *Daily cycle of the latent heat flux (a) and sensible heat flux (b) at 15 June 2010, as measured and modeled by the single-column model at Cabauw. Obs H is the observed sensible heat flux, Obs H + Res is the residual term added to this.*

On non-heat wave days the cycles of the turbulent fluxes are well captured by the model (Figure 3.8 for a typical summer day), but sensible heat flux only agrees with the observations when the whole residual term is consired to be sensible heat flux (green points).

Agreement model and observations
We have seen that the model captures the general dynamics of the temperature, precipitation, radiation and turbulent fluxes. However, it is biased warm and dry, leading to too high air temperatures, too little rain and cloud formation and an overestimation of the Bowen ratio. This bias is particularly present on heat wave days.

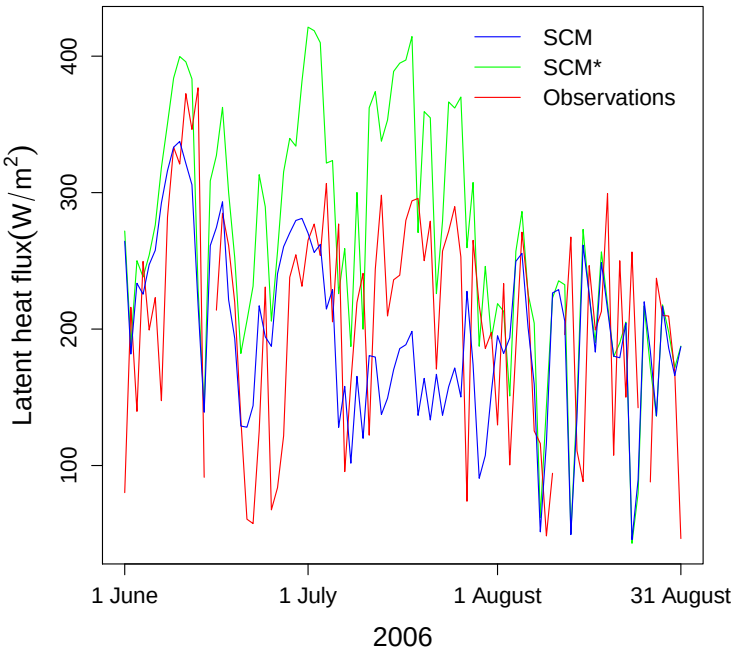

Figure 3.9: *Mean 9-13 UTC latent heat flux in the summer of 2006, as measured and modeled by the SCM at Cabauw with normal soil moisture progression (SCM) and with the soil moisture content kept at field capacity (SCM*).*

An explanation could be that the ground water level at Cabauw is manually managed by the local water board. Groundwater can influence soil moisture and thereby surface evapotranspiration (Chen and Hu, 2004). To test the sensivity of the SCM to soil moisture, an extra run is done with the soil moisture content kept at field capacity (SCM*).

On normal days, the Bowen ratio of SCM* is 0.39, which is much closer to the observations than the original SCM run (Table 3.2). On heat wave days, when the soil tends to be dry, the net radiation is higher than the original run because of lower surface temperatures. Most of the additional energy is spend

on latent heat flux (100 Wm^{-2} increase, while 1 Wm^{-2} for sensible heat flux). The increase of net radiation and the decrease of the Bowen ratio is larger than the observations and represents an upper bound as actual soil moisture content will be somewhere between the one modeled by the SCM and field capacity. This results in the actual latent heat flux lying inbetween SCM and SCM* (Figure 3.9).

This enforces the idea that manual groundwater management is the probable cause of the deviations of the model from the observations. As the difference between forest and grassland is the focus of this thesis and not the actual situation at Cabauw, we conclude that the SCM performs well and is suitable for the research.

3.1.2 SCM and TESSEL

The offline TESSEL runs were forced using the output of the RACMO SCM reference Cabauw run. We used albedo, 15 minute averaged rainfall rates, incoming longwave and shortwave radiation, temperature, wind and humidity values from the lowest model level and pressure from the lowest half level. All the initial conditions were the same as the initial conditions in the RACMO SCM run. As the Cabauw run of TESSEL is forced with the same atmospheric conditions as the land scheme of RACMO SCM in the reference Cabauw run, the output of both runs should be the same. Any differences that occur can be attributed to the version of TESSEL used offline being different from the one used in RACMO SCM (Section 2.3).

Net radiation
As incoming shortwave and longwave radiation were forcings and outgoing shortwave radiation was determined by the forced albedo, the net radiation difference between the SCM and TESSEL runs can only reside in rounding errors and outgoing longwave radiation.

TESSEL calculates 4 Wm^{-2} more net radiation during normal summer days (9-13 UTC mean), meaning less outgoing longwave radiation (Figure 3.2). This is a consequence of lower surface temperatures of about 0.1 K. During heat waves the surface temperatures in the TESSEL run drop compared to the SCM (difference of 0.3 K), so that the surface receives even more additional energy (Figure 3.3).

Turbulent fluxes
As a result of lower surface temperatures, TESSEL calculates less ground heat flux than the SCM. However, the boundary layer also becomes less stable because of lower temperatures near and at the surface. Atmospheric resistance is therefore decreased so that it still calculates higher sensible heat flux. The extra net radiation in the TESSEL run is spend on latent heat flux, which is 4 Wm^{-2} higher than RACMO SCM calculates.

During heat waves, surface temperatures are lower in the TESSEL run. Still the Bowen ratio is higher, again because of decreased stability of the boundary layer. Ground heat flux increase is smaller, as expected from the surface temperatures.

Agreement SCM and TESSEL
We conclude that surface temperatures are lower in TESSEL than those calculated by RACMO SCM. Sensible heat flux is always higher and ground heat flux always lower in TESSEL, while latent heat flux is higher during normal summer days and lower during heat wave days. The deviation is in the order of only a few Wm^{-2} but should be considered in the analysis of the forest and grass runs.

3.2 Integrated energy response to heat waves

Output of RACMO SCM for the period 2005-2011 showed that using grassland as vegetation, Cabauw experienced three heat waves during this time. The first was from 18 June to 25 June 2005 (8 days), the second from 10 July to 30 July 2006 (21 days), the third from 7 July to 15 July 2010 (9 days). Using forest as vegetation yielded these three heat waves and another two: 9 June to 14 June 2006 (6 days) and 29 June to 7 July 2006 (9 days). During both these periods, temperatures over grassland were above 25° C. However, only one tropical day was recorded during the former period and only two during the latter. To make the comparison more fair, in the following analysis all five heat waves for forest are also taken to be heat waves for grassland.

The uncoupled TESSEL runs gave three heat waves: 18 June to 24 June 2010 (7 days), 30 June to 6 July 2006 (7 days) and 15 July to 27 July 2006 (13 days). The heat waves were the same for both vegetation types because air temperature was forced. It was, however, forced at the lowest model level (at approximately 6 m height) and not at 2 m height, so minor differences (0.3 K at the largest) in 2m air temperature occur. Also for the uncoupled runs, all five heat waves of the coupled forest run are taken to be heat waves.

For both vegetation types and both the coupled and uncoupled run, the flux climatology is calculated for all the terms in the SEB (Figure 3.10), by taking the mean over the normal (non heat wave) summer days. Again, the period 9.00-13.00 UTC is considered, when heating at the surface is maximal.

Incoming shortwave and longwave radiation are forcings, but are affected by cloud cover. Their climatalogies differ only marginally between all runs. Forest has a lower albedo than grassland, and therefore reflects less shortwave radiation. This is only partly counteracted by increased longwave radiation emittance, so that forest receives more net radiation. In the uncoupled runs net radiation is increased for both forest (by 4 Wm^{-2}) and grassland (by 3 Wm^{-2}). The extra energy received by forest in comparison to grassland is spend mostly on sensible heat flux and ground heat flux, which is an indication of higher surface temperatures. Grassland loses more energy via latent heat flux. The Bowen ratios of 0.82 for forest and 0.56 for grassland in the SCM run are increased to 0.87 and 0.59 for the uncoupled runs (Table 3.3). This means that the additional energy received by the surface in the uncoupled runs is lost via sensible heat flux. Also the ground heat flux is increased.

The heat wave day anomaly is calculated as the difference between the 9.00-13.00 UTC mean over the heat wave days minus the climatology (Figure 3.11).

Again, incoming radiation values are similar for all runs. The outgoing radia-

tion shows the same behaviour as for the climatalogies: less shortwave radiation reflected and more longwave radiation emitted by forest and the difference in net radiation increased in the uncoupled run. Most of the additionally received energy on heat wave days is used for sensible heat release by forest, while grassland tends to increase its latent heat release more. In the SCM runs, the Bowen ratios of the energy increase during heat wave days are 3 and 1.08 for forest and grassland respectively. Also, forests use more additional energy for ground heat flux. The Bowen ratios of the energy increase during heat wave days are 3.3 for forest and 1.77 for grassland in the uncoupled runs. The ratio of forest over grassland of the Bowen ratio is larger for the coupled runs, so the difference between forests and grassland in energy response to heat waves is enlarged in these runs. The cause for this, which should reside in land atmosphere feedbacks, is investigated in the next sections.

Table 3.3: *Bowen ratios of the climatology and the HWD anomaly for the forest and grassland runs and the ratio of forest over grassland (f/g) of the SCM and TESSEL.*

		Climatology	HWD anomaly
RACMO SCM	forest	0.82	3.0
	grassland	0.56	1.08
	f/g	1.46	2.78
TESSEL	forest	0.87	3.3
	grassland	0.59	1.77
	f/g	1.47	1.86

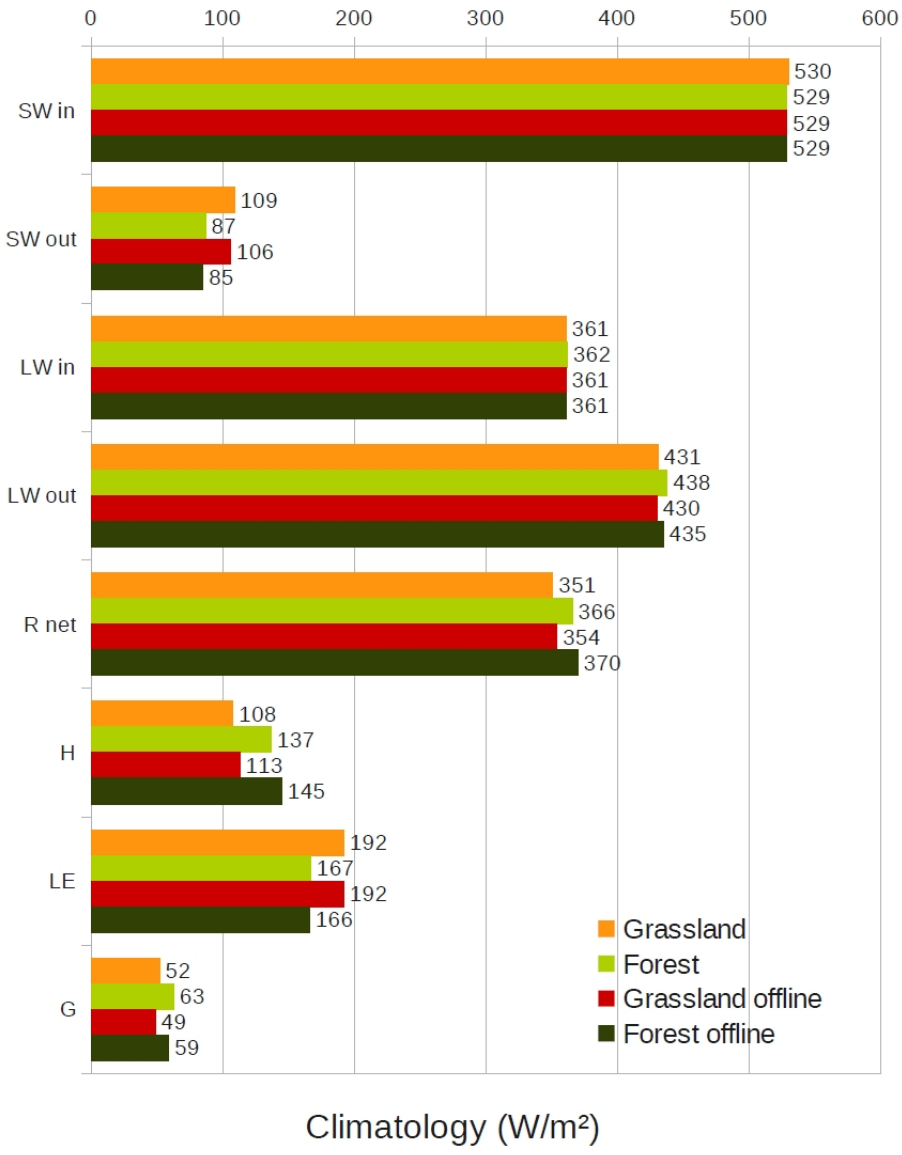

Figure 3.10: *Summer 9-13 UTC mean flux climatology over 2005-2011 for the terms in the SEB.*

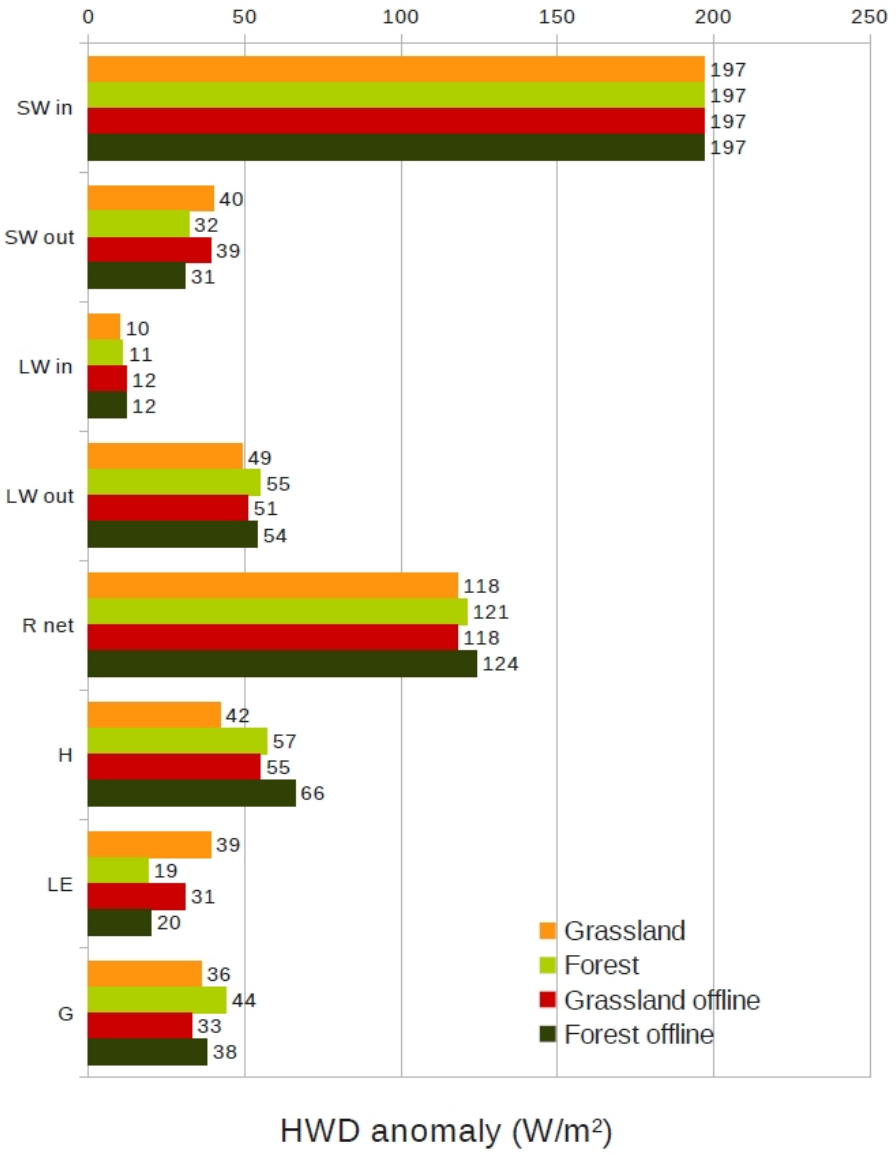

Figure 3.11: *Summer 9-13 UTC heat wave anomaly for the terms in the SEB.*

3.3 Daily evaporation cycle

3.3.1 Forcings and feedbacks

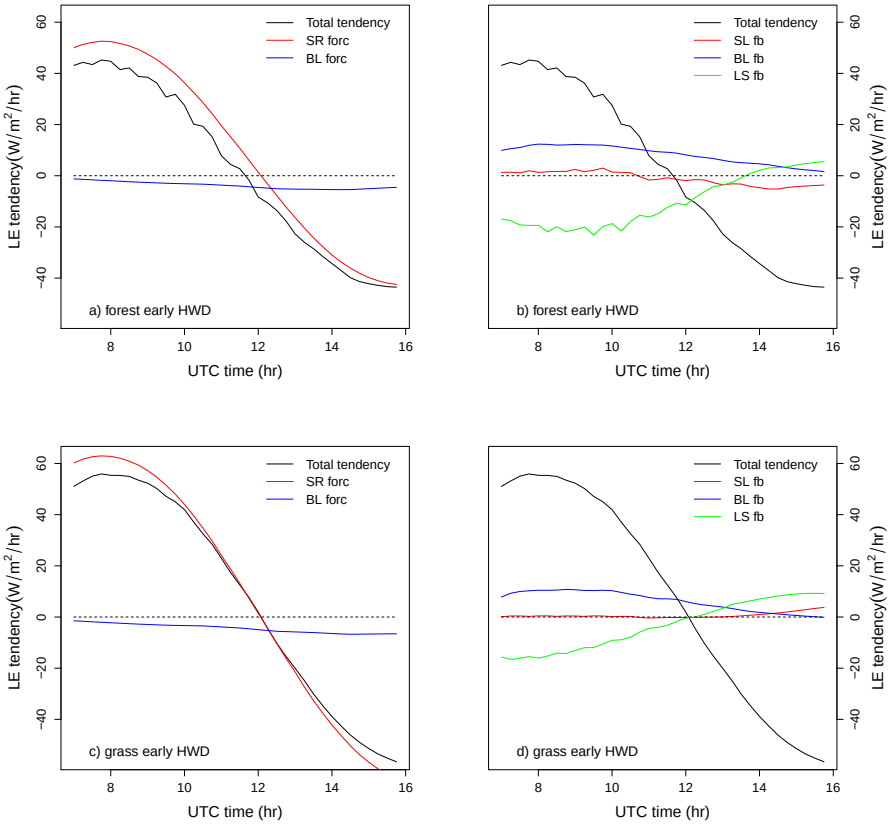

Figure 3.12: *Contributions of the forcings (a) forest, c) grassland) and feedbacks (b) forest, d) grassland) to the total surface evaporation tendency for early heat wave day 19 June 2005. (SR forc = surface radiation forcings, BL forc = boundary layer forcings, SL fb = surface layer feedback, BL fb = boundary layer feedbacks and LS fb = land surface feedbacks, similar in Figures 3.14 and 3.15)*

The different forcings and feedbacks in the Van Heerwaarden equation are plotted for the nearly cloudless heat wave day 19 June 2005 (Figure 3.12). This was a day in the beginning of the 2005 heat wave. The most apparent difference between grassland and forest response to heat waves and accompanying drought resides in the surface radiation forcings.

The surface radiation forcing is the main driver of evapotranspiration. It makes a cycle, acting positively in the morning when the sun comes up, gradualy decreasing until 12.00 UTC. At this moment, the sun starts going down and the surface radiation forcing becomes increasingly negative. The amplitude of this cycle is smaller for forest than for grassland. This is determined by the surface resistance, which impacts on c_0 (Figure 3.13a).
The surface resistance is much higher for forests and evolves over the day, sim-

ilar to the semi-arid Niamey case in Van Heerwaarden et al. (2010). In the grassland case we recognize the evolution of a mid-latitude surface resistance. Forest reacts more heavily to the increased VPD via f_3 in Equation 2.13, which reaches values up to 2.6. f_3 is defined 1 for grassland, as g_d is zero.

This difference is only partly counteracted by the soil moisture content. Forest evaporates less, so it generally has a higher soil moisture content, which leads to less surface resistance via f_2 in Equation 2.13 (Figure 3.13b).

The boundary layer forcings are unimportant on this day as advection of heat and moisture was very small.

Also the surface layer feedback plays only a minor role in both cases. Most of the day values range between -1 and 1 W/m^2/hr. Values up to 4 W/m^2/hr for grassland and -4 W/m^2/hr for forest are reached only late in the afternoon. This small sensitivity of the evapotranspiration to aerodynamic resistance in the coupled land-atmosphere system is in accordance with the findings of McNaughton and Spriggs (1986).

The boundary layer feedbacks and land surface feedbacks remain to be analysed in the next sections.

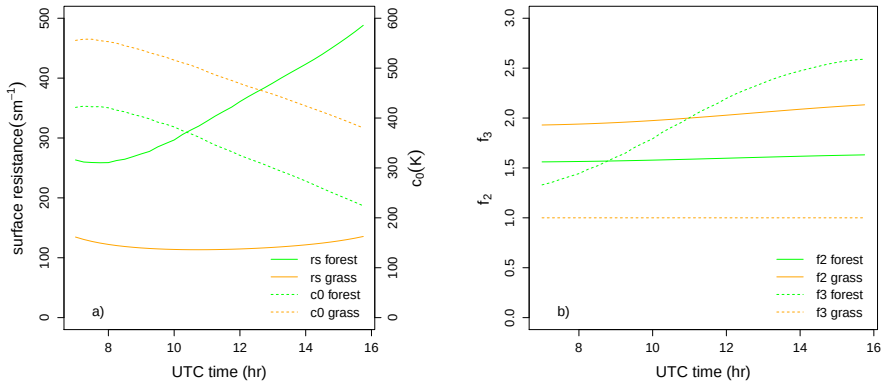

Figure 3.13: *Time evolution of surface resistance and c_0 (a) and f_2 and f_3 in Equation 2.13 for forest and grass on 19 June 2005.*

On the nearly cloudless normal (non-HWD) summer day 15 June 2010, the terms in the Van Heerwaarden equation generally follow the same behaviour (Figure 3.14) . However, their values are much smaller. The surface receives less incoming radiation. Maximum values for surface radiation forcing reach only up to 25 W/m^2/hr for the forest case and 40 W/m^2/hr for the grassland case. This difference is caused by the surface resistance being larger in the forest case, since the factor $\frac{r_{s,min}}{LAI}$ in Eq. 2.13 is larger (Table 2.1). Less forcing also leads to less feedback. The absolute influence of the feedbacks is diminished (see Section 3.3.2 and 3.3.3). Boundary layer forcing is now an important term. Evapotranspiration is pushed down by advection of cold and moist air, particularly in the afternoon.

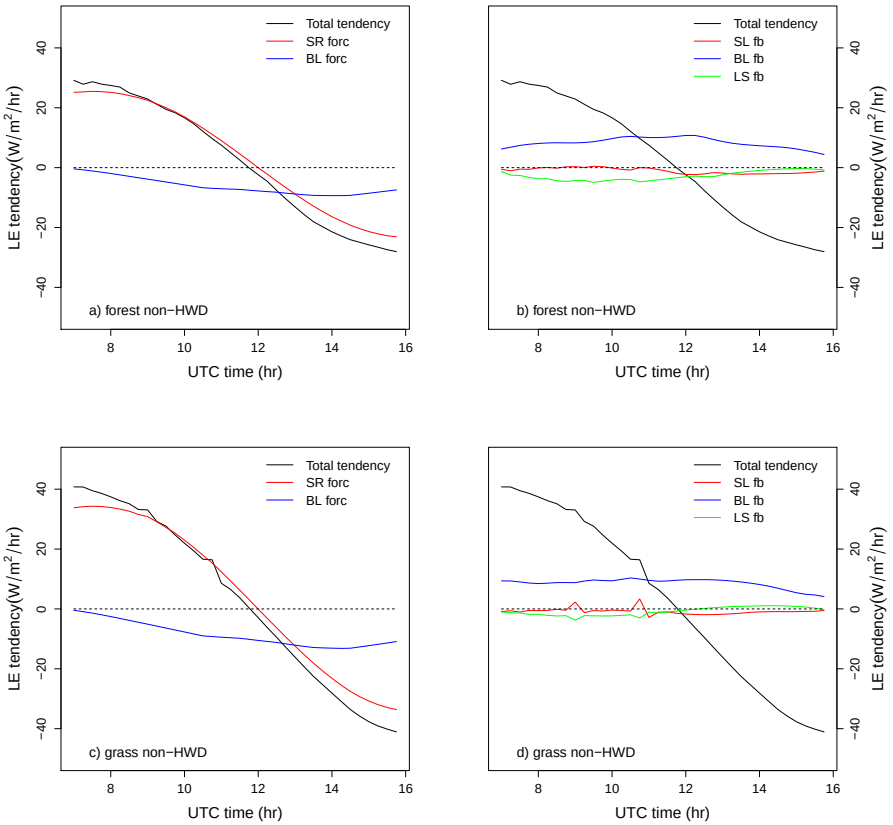

Figure 3.14: *Contributions of the forcings (a) forest, c) grassland) and feedbacks (b) forest, d) grassland) to the total surface evaporation tendency for non-heat wave day 15 June 2010.*

21 July 2006 was a day at the end of the heat wave of 2006. Analyzing the forces and feedbacks in the Van Heerwaarden equation (Figure 3.15) we notice that the difference with the early heat wave day 19 June 2005 is mainly caused by different forcings.

The surface radiation forcing is less strong in both the forest and the grassland case. The incoming radiation values being about equally large on both days, this weaker forcing is because the surface resistance is much higher (Figure 3.16a) and this impacts on c_0. The increased surface resistance is only a consequence of lower soil moisture content, as VPD values are smaller during this day.

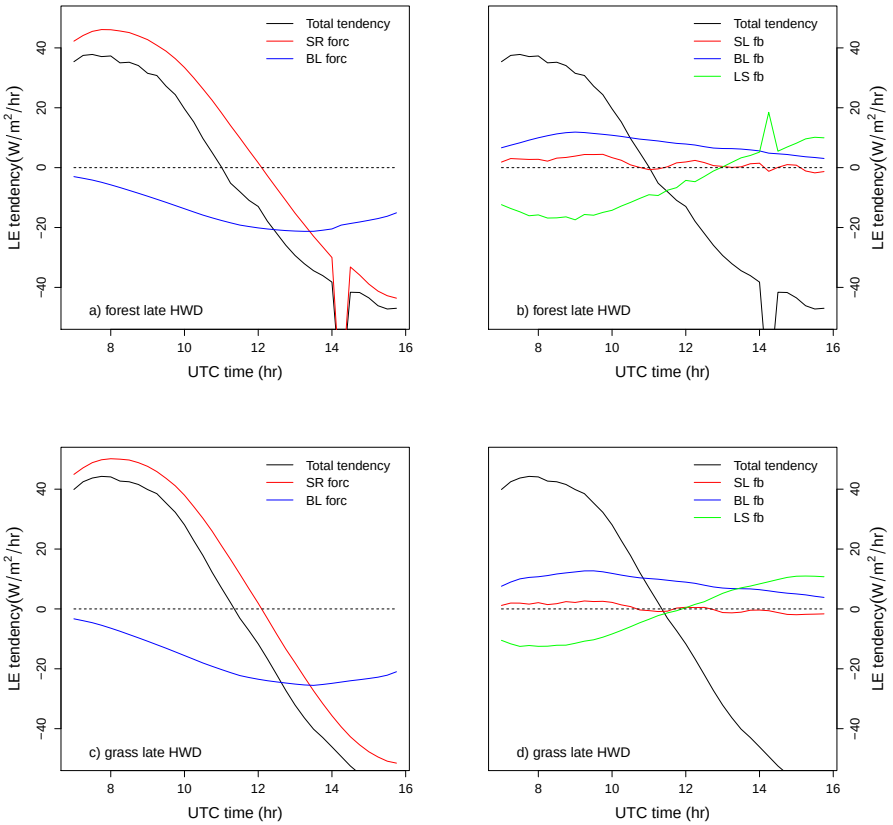

Figure 3.15: *Contributions of the forcings (a) forest, c) grassland) and feedbacks (b) forest, d) grassland) to the total surface evaporation tendency for late heat wave day 21 July 2006.*

The boundary layer forcing on the other hand is much larger because of stronger winds, pushing the evapotranspiration tendency down.

Also on this day the surface layer feedback had a negligible impact, albeit somewhat larger in the morning than on the early heat wave day. Since c_0 is smaller, this implies that the aerodynamic resistance rises more steeply in the morning (Figure 3.16b, for the forest case). The growth of r_a is enlarged by a bigger difference between the surface temperature and the temperature of the atmosphere (Liu 2007). On the early heat wave day this difference reaches values up to 5 K for grassland and 8 K for forest, while on the late heat wave day values go up to 9 and 10 K for grassland and forest respectively.

The boundary layer feedbacks and land surface feedbacks are similar to the early heat wave day, and we will analyze them further in the next sections.

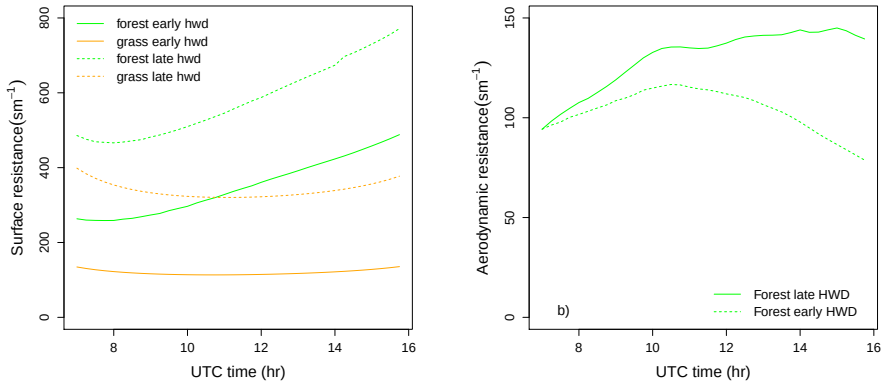

Figure 3.16: *Time evolution of surface resistance for forest and grass (a) and aerodynamic resistance (b) for forest on early heat wave day 19 June 2005 and late heat wave day 21 July 2006.*

3.3.2 Boundary layer feedbacks

Focusing on the boundary layer feedbacks (Figure 3.17), we see that because forest releases more sensible heat than grassland, in a relative sense the surface warming feedback ($H \uparrow\rightarrow \theta \uparrow\rightarrow LE \uparrow\rightarrow H \downarrow$) is more important for forest. Because forest evaporates less, the surface evaporation feedback ($LE \uparrow\rightarrow q \uparrow\rightarrow LE \downarrow$) is more important for grassland. In absolute sense the surface warming feedback is about equally large for both cases, due to c_0 being larger for grassland. On the early heat wave day both feedbacks are very strong in the morning, gradually declining (becoming less negative in the surface evaporation feedback case) during the day. This is because the released heat and moisture has to be distributed over an increasingly high boundary layer (see Figure 3.18a). During normal summer conditions the boundary layer shows a relatively modest growth, starting at higher values, so that the feedbacks remain about equally important throughout the morning, only decreasing in the late afternoon when the sensible heat flux and the latent heat flux decline.

The effect of boundary layer growth is also visible in the progress of the entrainment fluxes. On the early heat wave day they are very strong in the morning and decline quickly, while on the normal summer day they already start at low values.

While forest entrains more air then grassland, the entrainment drying feedback is less important. The explanation is twofold: 1) The boundary layer is higher than for grassland, 2) the temperature is higher than in the grassland case. A higher boundary layer implies that the effects of entrained air are reduced. This is particularly important on the normal summer day and in the afternoon of the heat wave day. A higher temperature impacts on evapotranspiration by non-linearly increasing q_{sat}, thereby increasing $\frac{dq_{sat}}{dT}$ (Figure 3.18b). This amplifies the temperature related processes (Equation 2.24), so they become more important relative to the processes related to humidity. Similar to the findings of van Heerwaarden et al. (2009) we find that at higher temperatures dry air entrainment becomes relatively less important.

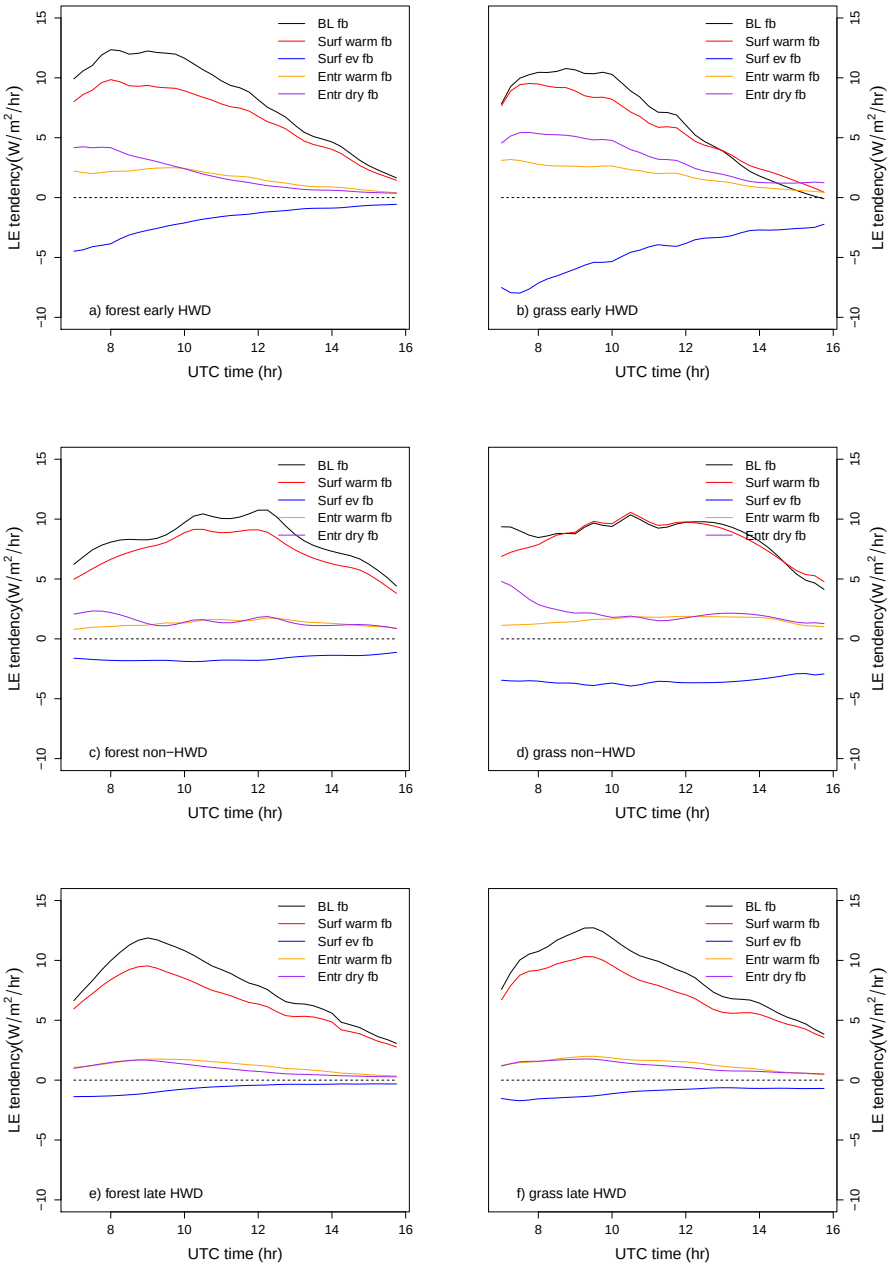

Figure 3.17: *Boundary layer feedbacks for forest (left) and grassland (right) on early heat wave day 19 June 2005, non-heat wave day 15 June 2010 and late heat wave day 21 July 2006. (BL fb= boundary layer feedbacks, Surf warm fb = surface warming feedback, Surf ev fb = surface evaporation feedback, Entr warm fb = entrainment warming feedback, Entr dry fb = entrainment drying feedback)*

The overall effect of the feedbacks is that the boundary layer feedbacks of grassland and forest look similar. On the early heat wave day they start at about 12 W/m^2/hr and gradually drop to zero throughout the day. On the normal summer day they increase from 5 W/m^2/hr to 10 W/m^2/hr during the morning and decrease back to 5 W/m^2/hr during the afternoon.

The boundary layer feedbacks for forest and grassland during the late heat wave day 21 July 2006 also look similar. However, the composition is very different.

While sensible heat flux is larger, the surface warming feedback is smaller on the late heat wave day. This is due to a smaller c_0. Relative to the other boundary layer feedbacks it is more important on the late heat wave day.

Latent heat flux is smaller on the late heat wave day, so the surface evaporation feedback is diminished. Also the difference between the forest case and the grassland case is smaller.

Since air temperatures on the late heat wave day are higher for both forest and grassland than on the early heat wave day, dry air entrainment has less influence. This is particularly notable in the grassland case.

Entrainment of warm air gives a similar contribution on both days, as boundary layer growth is comparable in magnitude.

Different contributions adding up to similar totals for boundary layer feedbacks was also noticed by Van Heerwaarden et al. (2010) who compared evapotranspiration in moist conditions (Cabauw) to semi-arid conditions (Niamey, Niger).

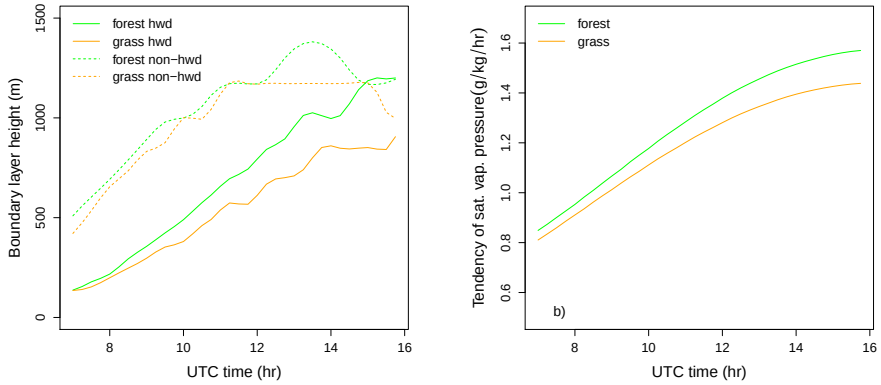

Figure 3.18: *Time evolution of boundary layer height on early heat wave day 19 June 2005 and late heat wave day 21 July 2006 (a) and the tendency of satuaration vapour pressure on early heat wave day 19 June 2005 (b) for forest and grassland.*

3.3.3 Land surface feedbacks

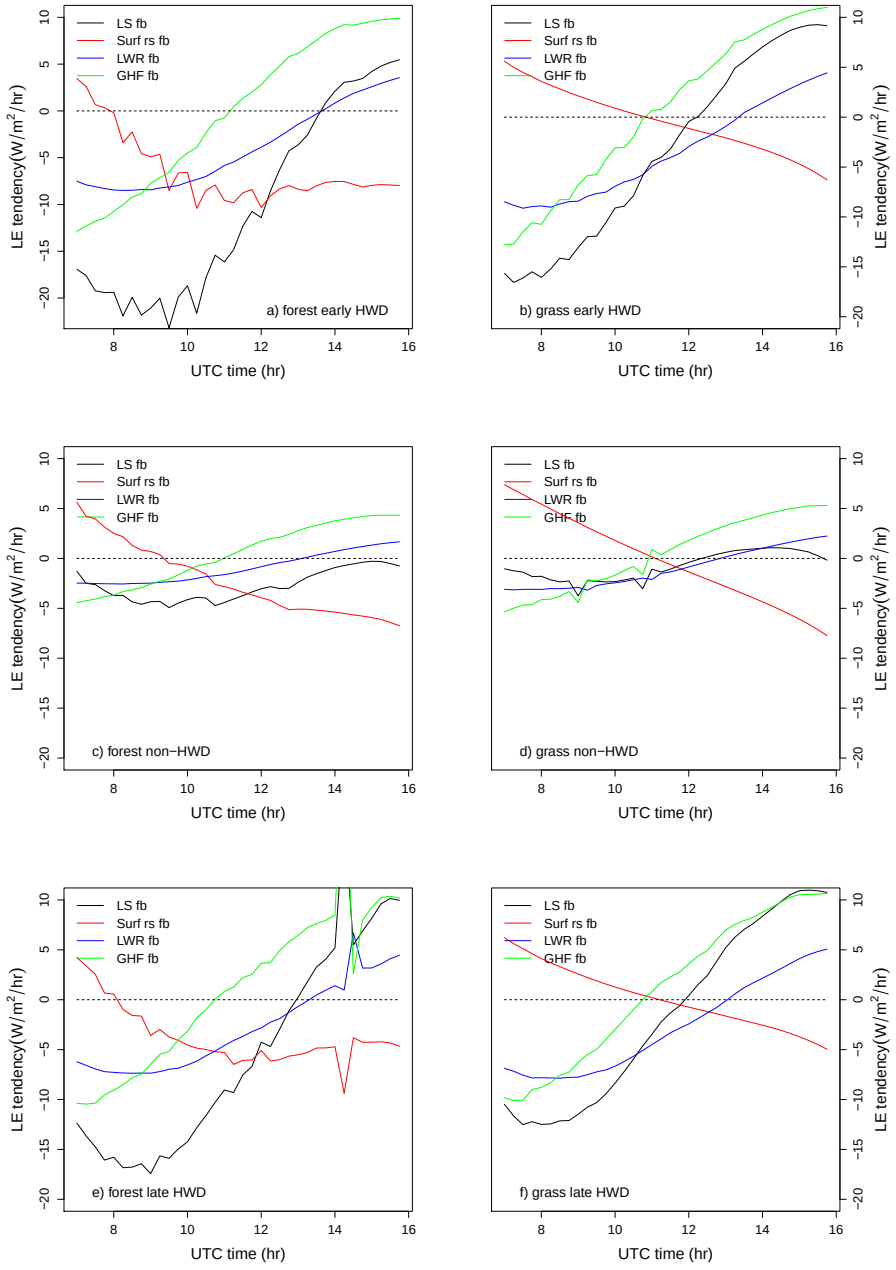

Figure 3.19: *Land surface feedbacks for forest (left) and grass (right) on early heat wave day 19 June 2005, non-heat wave day 15 June 2010 and late heat wave day 21 July 2006. (LS fb = land surface feedbacks, Surf rs fb = surface resistance feedback, LWR fb = long wave radiation feedback, GHF fb = ground heat flux feedback)*

An analysis of the different land surface feedbacks during heat wave days and non heat wave days over grassland and forests (Figure 3.19) learns us that the surface resistance feedback is a main factor, contributing to the energy balance difference between grassland and forest. This difference is larger on the heat wave day then on the normal summer day.

For grassland, the surface resistance decreases during the morning and increases during the afternoon, under influence of f_1 in Equation 2.13 (Figure 3.16a). This results in a approximately linearly decreasing surface resistance feedback, acting positively on evapotranspiration in the morning and negatively in the afternoon. The difference between a heat wave day and a normal summer day is small relative to the same difference for forest. The amplitude of the cycle is somewhat larger on a normal summer day because then the surface resistance is smaller and consequently c_0 is larger.

For forest, the surface resistance starts increasing already at 8.00 UTC on the heat wave day, because of the increasing vapour pressure deficit (Figure 3.20) via f_3. This leads to the surface resistance being negative from 8.00 UTC onwards, severely lowering the total of the land surface feedbacks. On the normal summer day the vapour pressure deficit is much smaller. This leads to a surface resistance feedback cycle looking more like the one of grassland, though values are still lower.

The long wave radiation feedback and ground heat flux feedback are almost similar in both cases. They tend to counteract surface radiation forcing, as these processes use available energy, that can then not be used for evaporation. On a normal summer day such as 15 June 2010, less energy from incoming short wave radiation is available. Hence, long wave radiation and ground heat flux will be smaller. This results in smaller long wave radiation and ground heat flux feedbacks. Again, these feedbacks are almost the same for grassland and forest.

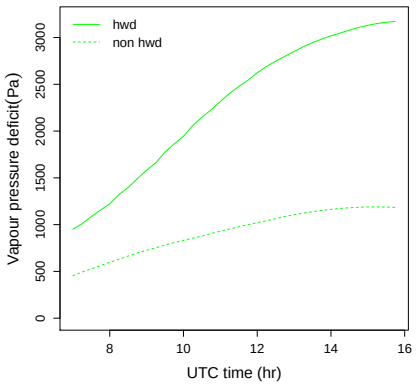

Figure 3.20: *Time evolution of vapour pressure deficit on early heat wave day 19 June 2005 and non-heat wave day 15 June 2010 for forest.*

The land surface feedbacks do not show a large difference between the early heat wave day and the late heat wave day. While one might expect increased surface resistance, because of drier vegetation and increased VPD, we see that

the surface resistance feedback is smaller on the late heat wave day. Two factors contribute to this. Firstly, while the surface resistance is larger in both the forest and grassland case, the increase in the time derivative of surface resistance, though present, is considerably less. Secondly, the factors c_0, LE and $\frac{1}{r_a}$, together determining the amplitude of the surface resistance feedback (Eq. 2.24) are all smaller for the late heat wave day.

3.3.4 Total effect of forcings and feedbacks

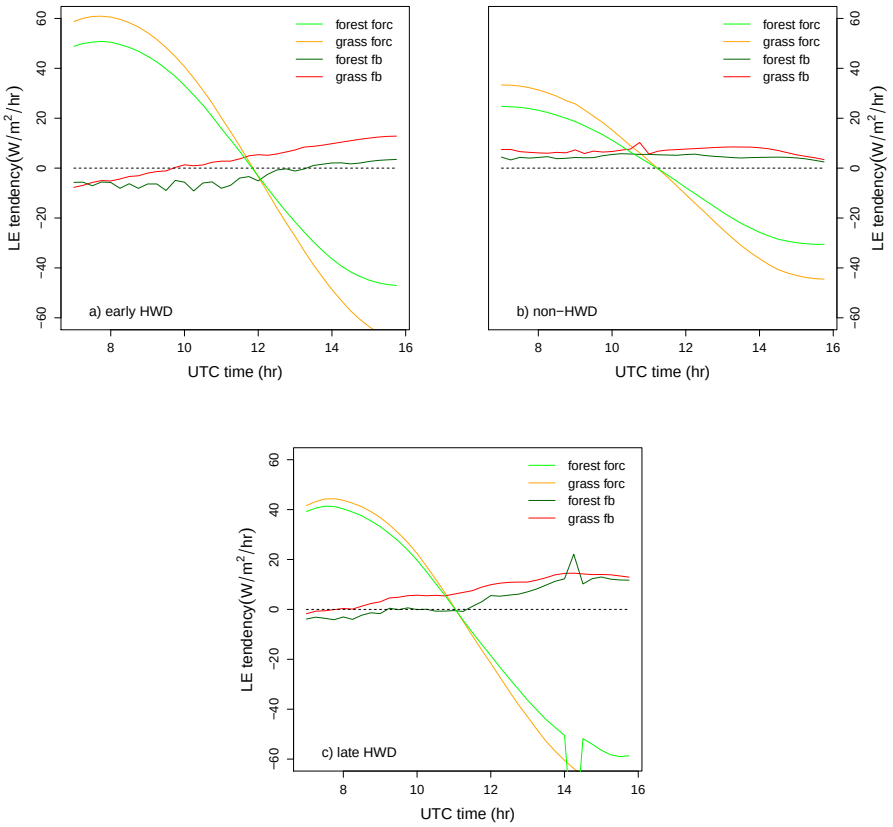

Figure 3.21: *Time evolution of boundary layer height on early heat wave day 19 June 2005 and late heat wave day 21 July 2006 (a) and the tendency of satuaration vapour pressure on early heat wave day 19 June 2005 (b) for forest and grassland.*

The combined effect of the forcings and the feedbacks is calculated for all the days analyzed in this section (Figure 3.21). The forcings are increased on the early heat wave day compared to the normal summer day. Also, the difference between grassland and forest grows. At the end of a heat wave, the forcings are smaller again because of higher surface resistance due to decreased soil moisture content. The difference between forest and grass also shrinks, because forest uses less water for evaporation during the beginning of the heat wave and so more water is available at the end.

The feedbacks are positive during the whole normal summer day. The boundary layer feedback is the main contributing feedback during this day. The total feedback is larger for grassland than for forest. This leads to more evapotranspiration in the grassland case, adding up to the difference induced by larger forcing in the grassland case that was already present.

On the early heat wave day the land surface feedback is very negative in the morning. The total feedback drops to negative values in the morning. The difference between forest and grassland increases, as the feedback for forest is more negative. The reason is the VPD function in Equation 2.13. Forest tends to increase its surface resistance during droughts (high VPD), while grassland is insensitive to VPD.

Late in the heat wave, grassland has evaporated more of its soil moisture than forest. This increases the water stress function in Equation 2.13. The difference in land surface feedbacks is consequently decreased. The outgoing long wave radiation, ground heat flux and the VPD are also decreased, increasing the land surface feedback in the morning, so that the total feedback is positive over most of the day for both grassland and forest.

In conclusion, the surface resistance feedback is the main factor that constitutes the different total feedback between the days and between the vegetation types. The difference in evapotranspiration between forest and grassland grows at the beginning of a heat wave, but becomes smaller as the heat wave progresses.

3.3.5 Effect of feedbacks on difference SCM and TESSEL

Land atmosphere feedbacks affect the difference between the latent heat flux of forest and grassland. This has consequences for the difference between coupled SCM modeling and offline land scheme modeling on the long term (Section 3.2), but also on the daily scale. We investigate the effect of the feedbacks on the early heat wave day 19 June 2005. One might expect that adding the value of the feedback difference to the difference calculated by TESSEL would give the results of the SCM, but the influence of the feedbacks is somewhat more complex than that (Figure 3.22).

All the terms in the Van Heerwaarden equation have gain factors. In the offline TESSEL runs, the atmospheric variables are altered in the same way for forest and grassland. However, after multiplication with the gain factor there is a difference in forcings and feedbacks, which subsequently affects the gain factors. The amplitude of the gain factor is decisive for the final difference in latent heat flux tendency between forest and grass in the SCM and TESSEL runs. The most important gain factor, present in all the terms, is c_0, which is a function of several variables (Equation 2.25).

First of these is the soil memory. The soil moisture content of the runs is different at the beginning of the day. This leads to a difference in function f_2 in Equation 3.12 and consequently to an altered surface resistance. On 19 June 2005 the difference in soil moisture between forest and grassland is smaller in the offline runs, leading to decreased f_2 difference. This results in a c_0 value for forest closer to that of grassland, so that the difference in latent heat flux tendency is decreased. As grassland tends to evaporate more, this difference is negative in the morning and positive in the afternoon. This means higher SCM-TESSEL tendency difference values in the morning and lower in the afternoon.

Setting the soil moisture content in TESSEL to the values of the SCM run every day at 0:00 UTC illustrates the effect of soil memory (see red dotted line in Figure 3.22).

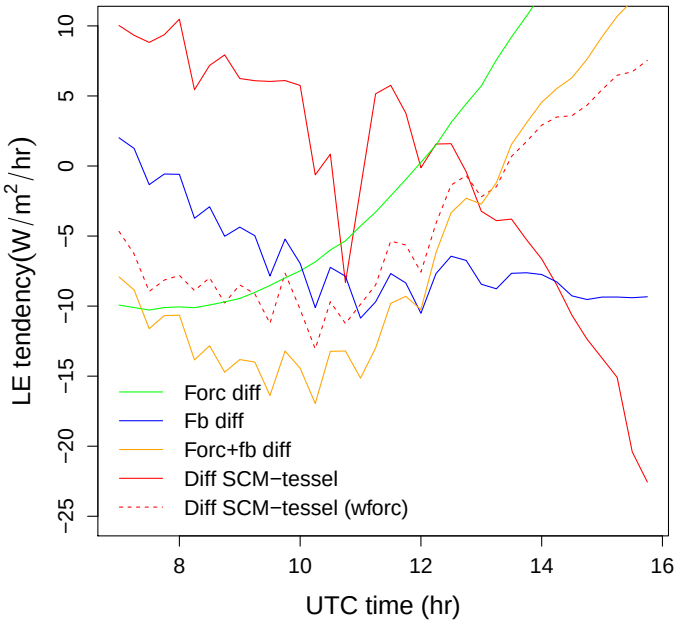

Figure 3.22: *Difference (SCM - TESSEL) of the latent heat flux tendency difference (forest - grassland) [Diff SCM-tessel] and difference in feedbacks (forest - grassland) [Fb diff], forcings [Forc diff] and forcings plus feedbacks [Forc+fb diff] on early heat wave day 19 June 2005. Wforc: soil moisture content of TESSEL set to SCM values at 0:00 UTC.*

Second, VPD influences the surface resistance (only of forest) via function f_3 in Equation 3.12. In the forest case, the VPD is larger in the offline TESSEL runs. Via a larger f_3 this leads to a decrease of c_0. This shifts the value further apart from grassland. The effect is the opposite from the soil moisture effect: lower tendency difference values in the morning and higher values in the afternoon.

The difference between SCM and TESSEL is furthermore influenced by contrasts in incoming radiation, resulting from different cloud cover (S_{in} and L_{in}) and surface temperatures (L_{in}). The combined influence of differences in forcings and feedbacks explains the bulk part of the difference between SCM and TESSEL (wforc) (see orange line in Figure 3.22). Finally, it is affected by the other gain factors (for instance dq_{sat}/dT in the surface radiation forcings).

In conclusion, to compare the feedbacks difference to the difference between latent heat flux tendency in SCM and TESSEL on a daily scale, the gain factors have to be considered and the soil moisture content of the offline runs has to be updated regularly. From this analysis, it is nonetheless clear that feedbacks have a severe impact on evapotranspiration on a daily scale, as their is a substantial difference between the forest-grassland contrast between SCM runs and TESSEL runs.

3.4 Differences in feedbacks, latent heat flux and atmospheric temperatures

3.4.1 Influence of feedbacks on the latent heat flux

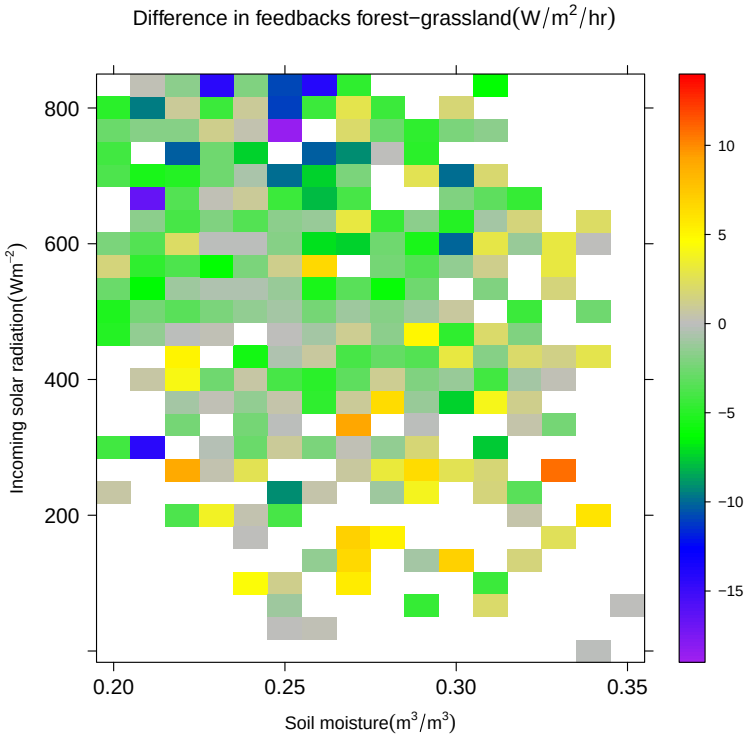

Figure 3.23: *Difference between the summer mean 9-12 UTC feedbacks in the Van Heerwaarden equation in the forest case and in the grassland case against the mean 9-13 incoming solar radiation and soil moisture of the Cabauw case.*

The effect of the feedbacks in periods of drought and high incoming solar radiation is different than on normal summer days (Section 3.3). Hence, feedbacks are affected by incoming solar radiation and soil moisture content. From the SCM runs, we calculate the difference in the integrated total feedback strength between forest and grassland. The integration is done over the time period 9.00-12.00 UTC, when heating is maximal and the sun is rising, so the tendency of the forcing is positive. The difference in feedback strength is displayed as a function of incoming solar radiation (9-13 UTC average, binned in 33 W/m^2 intervals) and soil moisture content (9-13 UTC average, binned in 0.01 m^3/m^3 intervals) of the reference Cabauw run (Figure 3.23).

Under normal summer conditions of 530 W/m^2 incoming solar radiation (see Figure 3.10), the feedbacks difference (forest minus grassland) is approximately -5 $W/m^2/hr$. This means that the latent heat flux of grassland increases relative to the latent heat flux of forest. The difference caused by the stronger forcing in the grassland case, is therefore increased by the feedbacks. In general the feedback difference becomes more negative with increasing incoming solar radiation and decreasing soil moisture content. The cause is that the surface

resistance in the forest case is increased by the VPD, which causes a stronger surface resistance feedback. However, when soil moisture content becomes very low (less then 0.25 m^3/m^3), the negative difference decreases. This is because the soil moisture content of grassland is smaller and the latent heat flux in this case is strongly reduced by the surface resistance, via function f_2 in Equation 2.13. As surface resistance is such an important factor, we expect the land surface feedbacks (via the surface resistance feedback) to be the most influential contributor to the total feedback difference.

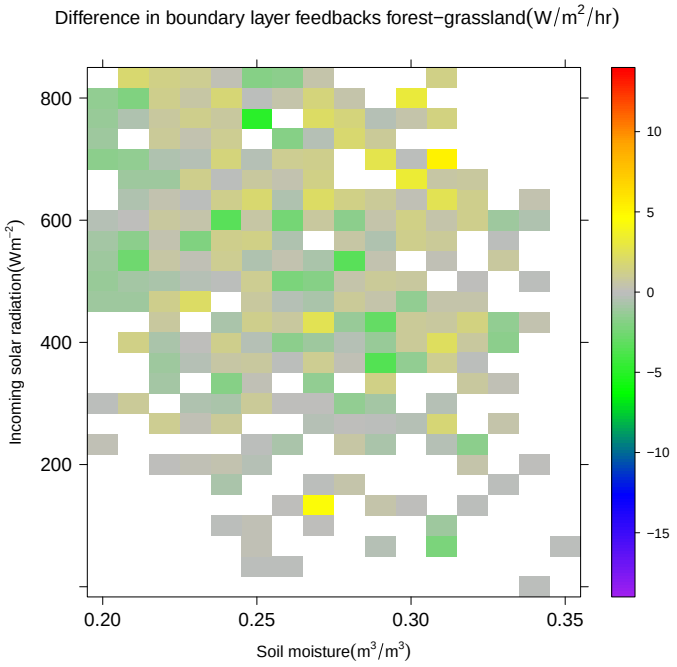

Figure 3.24: *Difference between the summer mean 9-12 UTC boundary layer feedbacks in the forest case and in the grassland case against the mean 9-13 UTC incoming solar radiation and soil moisture of the Cabauw case.*

Looking at the contributions of the different feedbacks to the total difference, we see the boundary layer feedbacks play only a small role with values ranging from -5 to 5 $W/m^2/hr$ (Figure 3.24). The effects of the different boundary layer feedbacks on the total forest-grassland difference tend to cancel each other out (Section 3.3.2). However, the total difference generally increases with increasing incoming solar radiation and soil moisture content. The reason is that forests evaporate less and this leads to less negative surface evaporation feedback and increased surface warming feedback.

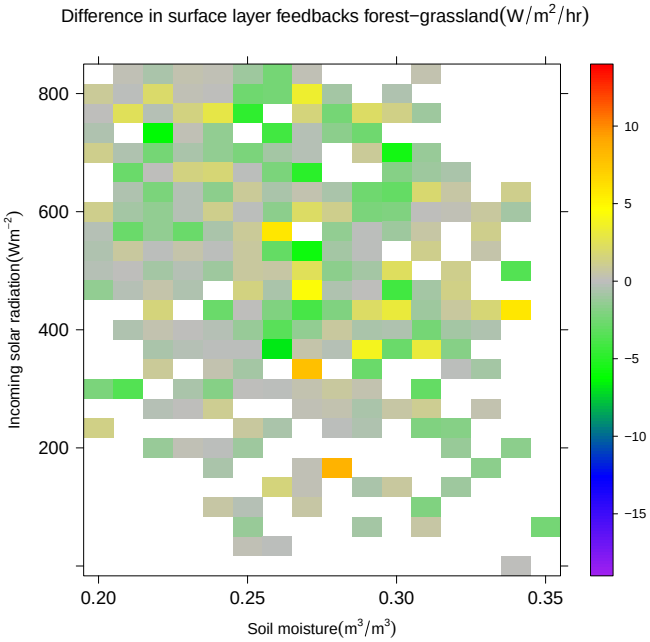

Figure 3.25: *Difference between the summer mean 9-12 UTC surface layer feedback in the forest case and in the grassland case against the mean 9-13 UTC incoming solar radiation and soil moisture of the Cabauw case.*

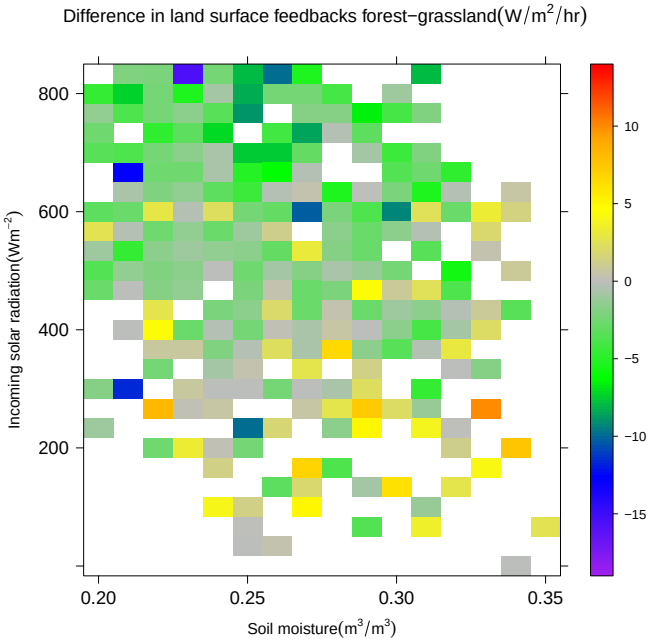

Figure 3.26: *Difference between the summer mean 9-12 UTC land surface feedbacks in the forest case and in the grassland case against the mean 9-13 UTC incoming solar radiation and soil moisture of the Cabauw case.*

The difference in surface layer feedback (Figure 3.25) shows a particularly noisy pattern and contributions are small (-5 to 5 $W/m^2/hr$).

As expected, the most important contribution is made by the land surface feedbacks (Figure 3.26). The pattern is similar to the total feedback difference, but the amplitudes are somewhat lower.

3.4.2 Influence of latent heat flux differences on atmospheric temperatures

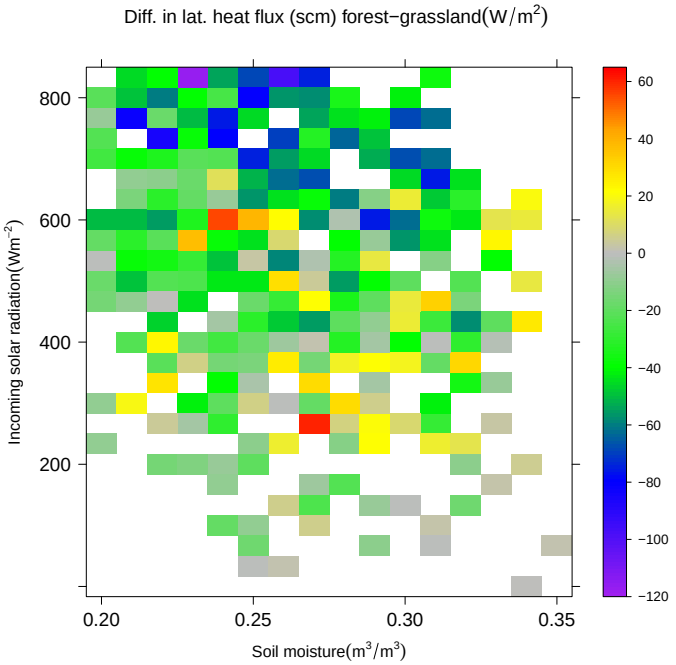

Figure 3.27: *Difference between the summer mean 9-13 UTC latent heat flux in the forest case and in the grassland case against the mean 9-13 UTC incoming solar radiation and soil moisture of the Cabauw case.*

The total latent heat flux difference is influenced by the differences in forcings and feedbacks. This difference is largest in conditions of high incoming solar radiation and low soil moisture content, but not so low that the water stress function (f_2 in Equation 2.13) becomes dominant in the difference in surface resistance between forest and grassland (Figure 3.27).

Via the surface energy balance, the difference in latent heat flux has an impact on atmospheric temperatures (Figure 3.28). When it becomes more negative, forest spends more energy on sensible heat release, heating up the atmosphere. Consequently, the atmospheric temperatures of forest are higher. The difference in 2m air temperature is approximately 1 K under normal summer conditions and reaches values up to 3 K in heat wave conditions (high incoming radiation values and modestly low soil moisture content). Hence, heat waves are generally more intense over forest.

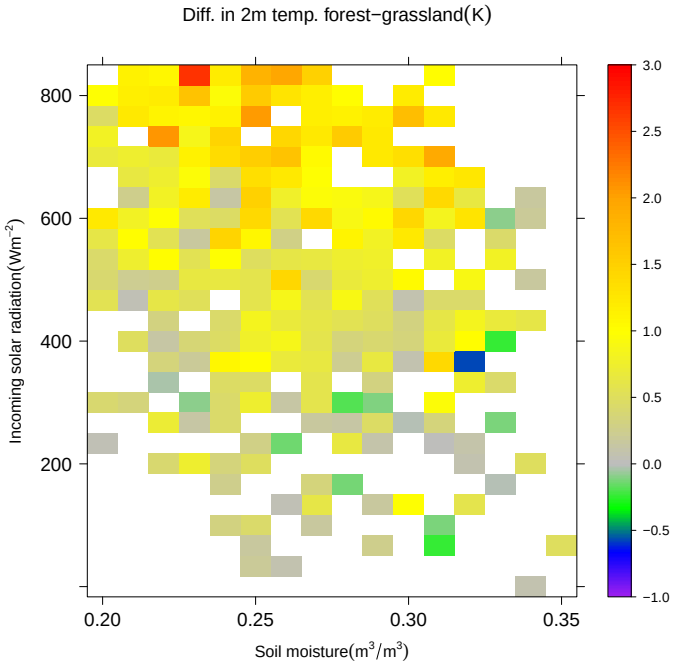

Figure 3.28: *Difference between the summer daily maximum 2m air temperature in the forest case and in the grassland case against the mean 9-13 UTC incoming solar radiation and soil moisture of the Cabauw case.*

Chapter 4

Conclusion

A conclusion, along with a discussion of the results and research perspectives, is presented in this Chapter.

4.1 Conclusion and discussion of the results

The modeled difference between the surface energy response of forest and grassland to heat waves is analysed by comparing coupled SCM runs to uncoupled land scheme runs for the period 2005-2011. The surface evaporation tendency equation developed by Van Heerwaarden et al. (2010), the Van Heerwaarden equation (Eq. 2.24), is used to determine the effects of the land atmosphere feedbacks on the difference in latent heat flux. First, three days, representing normal summer conditions, early heat wave conditions and late heat wave conditions, were investigated. Next, the feedback strengths were integrated over the 9-12 UTC time interval for the whole researched period.

Integration of the surface energy balance terms over the 9-13 UTC time interval showed that under normal summer conditions RACMO SCM and TESSEL calculate an almost equal difference in latent heat flux between forest and grass. TESSEL calculates slightly higher sensible heat fluxes than RACMO SCM, but the forest-grass difference remains the same.

On heat wave days, the difference in latent heat release between forest and grass is amplified in the results of both models. The latent heat release of grassland increases more than that of forest. Forest uses more of the excess energy on sensible heat release than grassland. However, this contrasting response is larger in the SCM runs, meaning that land atmosphere feedbacks increase the difference between forest and grassland during heat waves.

On the daily scale, from analyzing the SCM results we find that the main difference in evapotranspiration between forest and grassland is caused by the surface radiation forcings. Although both vegetation types are forced with the same radiation data, their gain factor c_0 differs substantially, primarily because of different surface resistances. The difference in surface resistance between forest and grassland becomes larger during heat waves. This is because the VPD is generally increased during heat waves and a higher VPD results in higher

surface resistance in the forest case. The forcing in this case is then less strong. At the end of a heat wave the soil moisture content of grassland has declined in relation to that of forest. This leads to a higher surface resistance in the grassland case. Now, the surface resistance and consequently the surface radiation forcings become more similar.

On all three days, the boundary layer feedbacks of forest and grassland give a similar contribution. This similarity is coincidental, as they are composed differently. Grassland has a more negative surface evaporation feedback, because its transpires more. This is counteracted by a more positive entrainment drying feedback, resulting from lower boundary layer height and lower near-surface temperatures. The total boundary layer feedback is only slightly higher during heat waves for both vegetation types, as the effect of the stronger surface warming feedback is reduced by the stronger, more negative, surface evaporation feedback.

The effect of surface layer feedback is negligible on all the days. The value of the aerodynamic resistance is determined by wind speed and the stability functions. Wind speed increases aerodynamic resistance and stabilizes the atmosphere. The stability functions are then decreased, leading to a decreased aerodynamic resistance. This negative coupling ensures that changes in aerodynamic resistance are only small, limiting the effect of the land surface feedback.

The difference in total feedback strength between forest and grassland is mainly determined by the land surface feedbacks. The longwave radiation feedback and ground heat flux feedback are almost similar in both cases, but the surface resistance feedback differs quite substantially. During normal conditions the surface resistance of forest is somewhat higher than that of grassland. This leads to a more negative surface resistance feedback in the morning, as evapotranspiration is suppressed more heavily. The difference grows during heat waves, because of the VPD dependence in the forest case. At the end of heat waves it shrinks, because the water stress (function f_2 in Equation 2.13) is much higher for grassland than for forest.

The land atmosphere feedbacks result in a different forest-grassland contrast, not only on the long term scale, but on the daily scale too. A simple addition of the feedback difference to the TESSEL results to get the SCM results is hindered by the gain factors in front of all the terms in the Van Heerwaarden equation. These gain factors are altered by the different forcings and feedbacks.

The difference in land atmosphere feedbacks between forest and grass has consequences for heat waves. In the coupled SCM runs, heat waves occurred more frequently over forest than over grassland. This is because atmopheric temperatures are generally higher in the forest case. During heat waves conditions (high incoming radiation, low soil moisture content) this temperature difference rises to about 3 K. This means that heat waves are also more intense over forest.

The earlier dry-out of grassland, discussed by Teuling et al. (2010), was also found, leading to decreased differences in evapotranspiration between forest and grassland at the end of heat waves. However, in none of the heat wave cases evapotranspiration of forest exceeded that of grassland. Also, heat waves over grassland did not last longer because of this dry-out. Lower soil moisture content for grassland is needed for that to happen.

4.2 Perspectives

Clouds

The feedback of evapotranspiration on cloud formation is not taken into account in the Van Heerwaarden equation. However, it is an important effect. Cloud cover can differ by as much as 60% between forest and grass (Figure 4.1). This can have a severe impact on the incoming radiation. Ek and Holtslag (2004) investigated the effect of the evaporative fraction ($LE/(H + LE)$) on relative humidity at top of the boundary layer. They found that it can be either negative or positive, leading to less or more cloud formation respectively, depending on a non-evaporative term. A cloud feedback may prove a worthy improvement of the Van Heerwaarden equation and needs to be researched further.

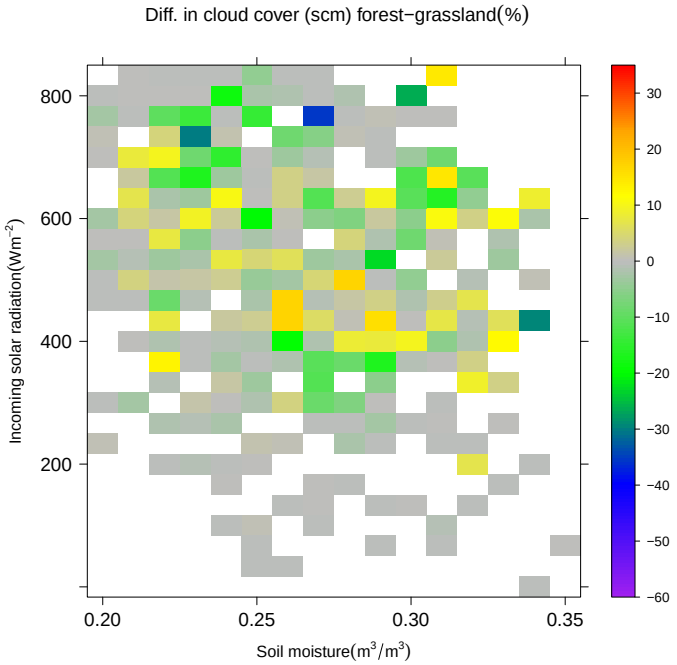

Figure 4.1: *Difference between the summer mean 9-13 UTC cloud cover in the forest case and in the grassland case against the mean 9-13 UTC incoming solar radiation and soil moisture of the Cabauw case.*

Soil drying

Soil moisture content is an important variable influencing evapotranspiration. The difference between the reference Cabauw run of the SCM and SCM*, in which soil moisture is set to field capacity at the beginning of each day, indicates that soil moisture limitation leads to considerably less latent heat release in normal summer conditions (224 W/m^2 to 185 W/m^2, Figure 3.2) and particularly on heat wave days (334 W/m^2 to 188 W/m^2, Figure 3.3). 2m air temperatures decline from 295.0 K to 294.3 K in normal summer conditions and from 302.6 K to 300.6 K on heat wave days, a difference of 2 K. All in all, groundwater management is largely influential on the climate of Cabauw.

Table 4.1: *Summer 9-13 UTC latent heat flux average (in* W/m^2*) for normal summer days and heat wave days in the TESSEL runs. Wforc: soil moisture content of TESSEL set to SCM values at 0:00 UTC.*

		TESSEL	TESSEL (wforc)
Climatology	forest	166	161
	grassland	192	193
HWD	forest	186	181
	grassland	223	235

The effect of soil drying is also illustrated by the difference between the offline TESSEL runs and the runs of TESSEL (wforc) with soil moisture content set to SCM values at the beginning of each day (Table 4.1). In the forest case, the soil is generally drier in the SCM runs than in TESSEL, as TESSEL (wforc) calculates less evapotranspiration. In the grassland case, TESSEL (wforc) calculates more evapotranspiration, which means that the soil is wetter in the SCM runs than in TESSEL. The effect of soil drying in this case is 12 W/m^2 in heat wave situations. Further research of the effect of soil drying on the long term time scale and on the daily scale is needed.

Acknowledgments

This thesis could not have been completed without the help and support of a few people. For his supervision of this research, I owe a big thank you to Bart van den Hurk. Roel Neggers deserves thanks for his co-supervision and all the help with the runs of RACMO SCM. Aarnout van Delden is thanked for second correction of the thesis. Fred Bosveld gave helpful insights on the soil moisture of Cabauw, thank you! Furthermore I'd liked to thank everybody at KNMI (in particular the land group) for their help and for making my internship an interesting and pleasant experience. Last but not least, I thank my friends and family for their moral support.

Bibliography

[1] Beljaars, A.C.M., 1991: Numerical schemes for parametrization. *Proc. of ECMWF Seminar on Numerical Methods in Atmospheric Models*, **2**, 1-42.

[2] Chen, X. and Q. Hu, 2004: Groundwater influences on soil moisture and surface evaporation. *J. of Hydrology*, **297**, 285-300.

[3] Ek, M.B. and A.A.M. Holtslag, 2004: Influence of soil moisture on boundary layer cloud development. *J.Hydrometeor.*, textbf5, 86-99.

[4] Foken, T., F. Wimmer, M. Mauder, C. Thomas and C. Liebethal, 2006: Some aspects of the energy balance closure problem. *Atmos. Chem. Phys.*, **6**, 4395-4402.

[5] Intergovernmental Panel on Climate Change (IPCC), 2007: Temperature extremes. *Climate Change 2007: Working Group I: The Physical Science Basis.*

[6] Jarvis, P.G., 1976: The interpretation of the variations in leaf water potential and stomatal conductance found in the field. *Phil. Trans. R. Soc. Lond. B.*, **273**, 593-610.

[7] Kelliher, F.M., R. Leuning, M.R. Raupach, E.-D Schulze, 1995: Maximum conductances for evaporation from global vegetation types. *Agricultural and Forest Meteorology*, **73**, 1-16.

[8] Lee, X., W. J. Massman and Beverly E. Law, 2004: Handbook of micrometeorology: a guide for surface flux measurement and analysis, *Kluwer Academic Publ., Dordrecht.*

[9] Lenderink, G. and A.A.M. Holtslag, 2004: An updated length-scale formulation for turbulent mixing in clear and cloudy boundary layers. *Q. J. Roy. Metorol. Soc.*, **130**, 3405–3427.

[10] Liu, S., L. Lu, D. Mao and L. Jia, 2007: Evaluating parameterizations of aerodynamic resistance to heat transfer using field measurements. *Hydrol. Earth Syst. Sci.*, **11**, 769-783.

[11] McNaughton, K.G. and T.W. Spriggs, 1986: A mixed-layer model for regional evaporation. *Bound.-Layer Meteor.*, **34**, 243-262.

[12] Monteith, J.L., 1965: Evaporation and environment. *Symp. Soc. Exp. Biol.*, **XIX**.

[13] Neggers, R. A. J., M. Koehler and A. A. M. Beljaars, 2009a: A dual mass flux framework for boundary-layer convection. Part I: Transport. *J. Atmos. Sci.*, **66**, 1465-1487.

[14] Neggers, R. A. J., 2009b: A dual mass flux framework for boundary-layer convection. Part II: Clouds. *J. Atmos. Sci.*, **66**, 1489-1506.

[15] Neggers, R.A.J., A.P. Siebesma and T. Heus, 2012: Continuous single-column model evaluation at a permanent meteorological supersite. *Bull. Amer. Met. Soc.*, Early Online Release.

[16] Seneviratne, S.I., T. Corti, E.L. Davin, M. Hirschi, E.B. Jaeger, I. Lehner, B. Orlowsky and A.J. Teuling, 2010: Investigating soil moisture-climate interactions in a changing climate: a review. *Earth-Sci. Rev.*, **99**, 125-161.

[17] Tennekes, H., 1973: A model for the dynamics of the inversion above a convective boundary layer. *Journ. of the Atmosph. Scs.*, **30**, 558-567.

[18] Teuling, A.J., S.I. Seneviratne, R. Stöckli, M. Reichstein, E. Moors, P. Ciais, S. Luyssaert, B. van den Hurk, C. Ammann, C. Bernhofer, E. Dellwik, D. Gianelle, B. Gielen, T. Grünwald, K. Klumpp, L. Montagnani, C. Moreaux, M. Sottocornola and G. Wohlfahrt, 2010: Contrasting response of European forest and grassland energy exchange to heatwaves. *Nature Geoscience*, **3**, 722-727.

[19] van den Hurk, B.J.J.M., P. Viterbo, A.C.M. Beljaars and A.K. Betts, 2000: Offline validation of the ERA-40 surface scheme. *ECMWF Tech. Memo. No. 295.*

[20] van Heerwaarden, C.C., J. Vilà-Guerau de Arellano, A.F. Moene, A.A.M. Holtslag, 2009: Interactions between dry-air entrainment, surface evaporation and convective boundary layer development. *Quart. J. Roy. Meteor. Soc.*, **135**, 1277-1291.

[21] van Heerwaarden, C.C., J. Vilà-Guerau de Arellano, A. Gounou, F. Guichard and F. Couvreux, 2010: Understanding the daily cycle of evapotranspiration: a method to quantify the influence of forcings and feedbacks. *J.Hydrometeor.*, **11**, 1405-1422.

[22] van Meijgaard, E., L.H. van Ulft, W.J. van de Berg, F.C. Bosveld, B.J.J.M. van den Hurk, G. Lenderink and A.P. Siebesma, 2008: The KNMI regional atmopheric climate model RACMO version 2.1. *KNMI TR 302.*

[23] van Ulden, A.P., and J. Wieringa, 1996: Atmospheric boundary layer research at Cabauw. *Bound.-Layer Meteor.*, **1-2**, 39-69.

[24] Wilson, K., A. Goldstein, E. Falge, M. Aubinet, D. Baldocchi, P. Berbigier, C. Bernhofer, R. Ceulemans, H. Dolman, C. Field, A. Grelle, A. Ibrom, B.E. Law, A. Kowalski, T. Meyers, J. Moncrieff, R. Monson, W. Oechel, J. Tenhunen, R. Valentini and S. Verma, 2002: Energy balance closure at FLUXNET sites. *Agricultural and Forest Meteorology*, **113**, 223-243.

[25] http://www.knmi.nl/ neggers/KPT/

[26] http://www.ecmwf.int/research/ifsdocs/

[27] http://www.knmi.nl/klimatologie/lijsten/hittegolven.html

[28] http://www.cesar-database.nl/